

AN ABSTRACT OF THE THESIS OF

Cody W. Ray for the degree of Master of Science in Mechanical Engineering presented on April 6, 2009.

Title: Modeling and Control of a Biologically Inspired Compliant Structure.

Abstract approved:

---

Belinda A. Batten

We hypothesize that the extraordinary maneuverability and efficiency of bats in flight are in part due to the compliant nature of their wing structures. We utilize the parameters of bat bones measured by biologists to create a biologically inspired model of a flapping system consisting of a rotating hub actuator and flexible Euler-Bernoulli beam. The problem of achieving flapping is formulated as an optimal control tracking problem. We investigate the solution to this problem using the Linear Quadratic Regulator (LQR), MINMAX, and linear quadratic gaussian (LQG) control methodologies. The success of each in rejecting a gust-like disturbance on the beam tip is investigated. It is shown that due to the mathematical formulation of the problem, the disturbance rejecting ability of MINMAX control is of little use to the types of disturbances investigated. LQG control is shown to be successful at rejecting the disturbance.

© Copyright by Cody W. Ray  
April 6, 2009  
All Rights Reserved

Modeling and Control of a Biologically Inspired Compliant Structure

by  
Cody W. Ray

A THESIS  
submitted to  
Oregon State University

in partial fulfillment of  
the requirements for the  
degree of

Master of Science

Presented April 6, 2009  
Commencement June 2009

Master of Science thesis of Cody W. Ray presented on April 6, 2009.

APPROVED:

---

Major Professor, representing Mechanical Engineering

---

Head of the School of Mechanical, Industrial, and Manufacturing Engineering

---

Dean of the Graduate School

I understand that my thesis will become part of the permanent collection of Oregon State University libraries. My signature below authorizes release of my thesis to any reader upon request.

---

Cody W. Ray, Author

## ACKNOWLEDGMENTS

I would like to thank Jeni for her help. I would also like to thank Dr. Belinda Batten and Dr. John Singler for their support and guidance throughout this project.

## TABLE OF CONTENTS

	<u>Page</u>
1 Introduction	1
2 Model Development	5
2.1 The Model . . . . .	5
2.2 Resulting Finite Element Approximation . . . . .	7
3 Flapping: An Optimal Control Tracking Problem	11
3.1 The Tracking Problem . . . . .	11
3.2 A Generalized Control Solution . . . . .	13
4 Simulations and Results	20
4.1 Model Problems . . . . .	21
4.2 Uncontrolled without a Disturbance . . . . .	22
4.3 Uncontrolled in the Presence of a Disturbance . . . . .	25
4.4 Regulation in the Presence of a Disturbance . . . . .	28
4.5 Tracking without a Disturbance . . . . .	31
4.6 Tracking in the Presence of a Disturbance . . . . .	34
5 Conclusions	36
Appendices	42
A Finite Element Derivation	42
B Simulations	51

## LIST OF FIGURES

Figure	Page
1.1 Simplified bat skeleton and flexible hub/beam model . . . . .	2
4.1 Tip force profile . . . . .	22
4.2 Uncontrolled beam tip deflection . . . . .	23
4.3 Uncontrolled hub angular position . . . . .	24
4.4 Uncontrolled hub angular velocity . . . . .	24
4.5 Uncontrolled system surface plot . . . . .	25
4.6 Uncontrolled/disturbed: Tip deflection . . . . .	26
4.7 Uncontrolled/disturbed: Hub angular position . . . . .	26
4.8 Uncontrolled/disturbed: Hub angular velocity . . . . .	27
4.9 Uncontrolled/disturbed: Surface plot . . . . .	27
4.10 Controlled/disturbed: Tip deflection . . . . .	28
4.11 Controlled/disturbed: Control exerted by hub . . . . .	29
4.12 Uncontrolled/disturbed: Hub angular position/velocity . . . . .	30
4.13 Tracking: Control torque . . . . .	32
4.14 Tracking: Hub angular position . . . . .	32
4.15 Tracking: Hub position tracking with greater control . . . . .	33
4.16 Tracking: System surface plot . . . . .	33
4.17 Tracking/disturbed: System surface plot . . . . .	34
4.18 Tracking/disturbed: Control . . . . .	35
B.1 Uncontrolled aluminum undisturbed . . . . .	52
B.2 Uncontrolled bone undisturbed . . . . .	53
B.3 Uncontrolled aluminum disturbed . . . . .	54
B.4 Uncontrolled bone disturbed . . . . .	55
B.5 Regulation bone disturbed - Control and hub position . . . . .	56
B.6 Regulation bone disturbed - Hub velocity and tip deflection . . . . .	57
B.7 Regulation bone disturbed - Surface plot . . . . .	58
B.8 Tracking/disturbed: Bone beam control and hub position . . . . .	59
B.9 Tracking/disturbed: Bone beam hub velocity and tip deflection . . . . .	60
B.10 Tracking/disturbed: Surface plots . . . . .	61

## NOTATION

$t$ :	Time ( $s$ )
$x, y, z$ :	Position coordinates ( $m$ )
$d(t, x)$ :	Vertical displacement ( $y$ direction) of the beam at time $t$ , position $x$ ( $m$ )
$v(t, x)$ :	Vertical velocity of the beam at time $t$ , position $x$ ( $m/s$ )
$\dot{d}(t, x)$ :	Time derivative of $d(t, x)$
$d_x, d_{xx}, d_{x..}(t, x)$ :	Spatial derivatives (with respect to $x$ ) of $d(t, x)$
$\theta(t)$ :	Angular position of the hub at time $t$ ( $radians$ )
$\omega(t)$ :	Angular velocity of the hub at time $t$ ( $radians/s$ )
$\rho(x)$ :	Density of the beam material at position $x$ ( $kg/m^3$ )
$A(x)$ :	Cross sectional area of the beam ( $m^2$ )
$I(x)$ :	Cross sectional moment of inertia of the beam at point $x$ ( $m^4$ )
$\gamma(x)$ :	Coefficient of Kelvin-Voigt damping at position $x$ ( $Ns/m^2$ )
$E(x)$ :	Young's modulus of beam at point $x$ ( $N/m^2$ )
$J$ :	Moment of inertia of the hub ( $Nm$ )
$I_m$ :	Moment of inertia of the tip mass $m$ ( $kg \cdot m^2$ )
$L$ :	Length of beam ( $m$ )
$L_m$ :	Length of the tip mass ( $m$ )
$m$ :	Mass at tip of beam ( $x = L$ ) ( $kg$ )
$f(t)$ :	Disturbance force upon beam tip at time $t$ ( $N$ )
$n_0$ :	Hub friction ( $Nm/s$ )
$\xi$ :	Minmax parameter

## 1 INTRODUCTION

Flapping flight is one of the most successful modes of animal locomotion. There are over 1,200 species of bats, 10,000 species of flying birds, and millions of species of flying insects [17]. The bat species specifically has found a unique balance between skeletal weight, strength, and functionality. As seen in Figure 1.1(a), even a greatly simplified schematic of a bat wing consists of many interconnected flexible bones. These compliant bones take on a connected form similar to that of the human hand, but taper towards the wing tip to reduce mass and exhibit much greater flexibility. The longest digits routinely experience bending deflections up to 30% of their length, respectively [14]. It is hypothesized that this flexibility, among other adaptations, is the primary reason bats are able to perform with seemingly unequalled flight capabilities in terms of both efficiency and aerodynamic performance [12]. This hypothesis suggests that incorporating flapping flight and compliant structures into micro air vehicle (MAV) design may lead to greater performance in such systems.

The multiple component structure (MCS) shown in Figure 1.1(b) was chosen to approximate the physiology of the single bat wing shown in Figure 1.1(a) for the purpose of investigating the characteristics and capability of typical control designs for a simple hypothetical flapping system. The MCS consists of three coupled structures. The first component is a rigid rotating actuator, through which a control input in the form of torque can be applied. This component represents a shoulder. Attached to the hub is a tapering rectangular Euler-Bernoulli beam of constant density, at the tip of which is another rigid body with a prescribed mass and geometry. Beam material parameters are consistent with bat wing bone geometry and physiology, and include Young's modulus and density estimates made by biologists in [12]. The tip mass was included in an attempt to generalize the system to model more complicated

structures, which may include an accelerometer sensor, allowing for the sensing of beam tip oscillations.

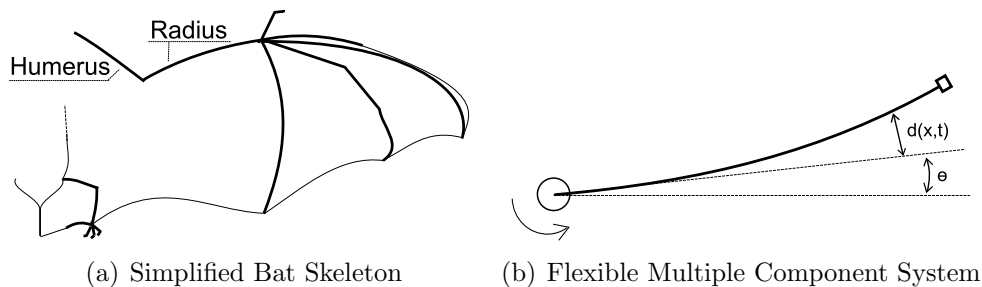


Figure 1.1: Simplified bat skeleton and flexible hub/beam model

Throughout this discussion, keep in mind that the chosen model is greatly simplified from any system that could achieve flapping flight. The purpose here is not to design and control a real flying model, but rather to investigate the use of optimal control theory in achieving flapping behavior in a simulated compliant system.

In this thesis, we pose the problem of achieving flapping behavior as a tracking problem. We compare the solutions obtained from linear quadratic gaussian (LQG) and  $H^\infty$  control methodologies in terms of tracking performance and robustness to disturbances, and thereby assess the potential of using such control schemes to control a flapping structure. We also compare these to the Linear Quadratic Regulator (LQR) solution.

In a flying system, there is always the possibility of a disturbance such as a gust of wind, turbulence, etc. With this in mind, we model a disturbance force upon the beam tip, which is always in the normal direction to the tip mass. We use this force to compare and contrast the disturbance rejection capability of the previously mentioned control schemes.

Relevant reviewed work involves fundamental methods applied to such flexible systems, and includes the finite element method, optimal control theory, and flapping

flight investigations. Finite element and optimal control theory are highly developed and are presented in detail in respective textbooks. A few related studies that offer deeper investigations into the theory of these topics are mentioned in the following review.

In [3], Gibson and Adamian investigated a very similar problem involving linear-quadratic-Gaussian (LQG) control of a flexible structure. Their model, however, did not taper, nor did it utilize biologically inspired material parameters. Equations approximating the system were developed using Hermite splines. They showed that the solution converged. They presented a guide to designing finite dimensional compensators that approximate the optimal compensator, which is found by solving the infinite dimensional Riccati equations. Furthermore, they stated that cubic B-splines (the method used in this thesis) require a larger approximation to achieve the same modal accuracy as Hermite splines.

Optimal control theory is very developed; almost every textbook on the subject discusses LQR, LQG, and MINMAX or  $H^\infty$  control. The control of flexible structures similar to the model presented in this thesis has been a subject of particular interest, especially in terms of vibration control. Much of the research conducted on vibration control has been dedicated specifically to the control of beam vibrations through the hub torque input. However, the author was unable to find a study in which flapping behavior of the system is achieved using such optimal tracking schemes. Most studies pertain to fluid-structure interaction of biological systems exhibiting flapping flight. More specifically, a multitude of studies in this research area are dedicated to the flight of insects, which is notoriously difficult to model and understand. Associated researchers at Brown University and MIT are working towards an understanding of such fluid-structure interactions during bat flight specifically [7, 8, 10, 11, 12, 13, 9, 15, 16, 17].

We were also unable to find any studies pertaining to the control of flapping beams with inhomogeneous parameters such as tapering geometry, and those with biologically inspired Young's modula and density.

Chapter two is a discussion of the physical model, the equations of motion of the model, and a finite dimensional approximation to the system of partial differential equations (PDEs) using the finite element method. In chapter three, we discuss the control theory, and the formulation of achieving flapping behavior as the solution to a tracking problem. Chapter four entails three generalized problems and the resulting simulations used to verify and compare the control schemes used.

## 2 MODEL DEVELOPMENT

This chapter contains the mathematical model of the MCS depicted in Figure 1.1(b). The equations of motion for this system were derived from the model for the more complicated structure found in [6], which was reduced from two beams rigidly connected to a single beam with tip mass, connected to a rotating hub. The resulting system of equations consists of a PDE relating hub and beam dynamics, four initial conditions for the hub and beam, and four boundary conditions relating hub/beam and beam/tipmass geometry and dynamics at the ends of the beam, respectively.

### 2.1 The Model

The PDE relating hub/beam dynamics is written as an Euler-Bernoulli beam equation with an additional inertial force term relating hub angular acceleration to beam mass and position. The equation includes the physical beam parameters such as density  $\rho(x)$  and the Kelvin-Voigt damping parameter  $\gamma(x)$ . In general, these parameters vary along the axial length of the beam. For our purposes, the density, Young's modulus, and Kelvin-Voigt damping parameters were fixed. Beam cross sectional area was made so that the beam becomes narrower towards the tip, so that it tapers in a manner similar to that found in bat bones. Thus, the terms  $A(x)$  and  $I(x)$  both vary with respect to the position variable  $x$ .

The Euler-Bernoulli beam equation,

$$\rho(x)A(x) \left( \ddot{d}(t, x) + x\ddot{\theta}(t) \right) + \left[ \gamma(x)I(x)\dot{d}_{xx}(t, x) + E(x)I(x)d_{xx}(t, x) \right]_{xx} = 0, \quad (2.1)$$

has four associated boundary conditions. The first two of which relate hub/beam

dynamics and a control input (torque on hub) at the point  $x = 0$ ,

$$J_0\ddot{\theta}(t) - \gamma(0)I(0)\dot{d}_{xx}(t, 0) - E(0)I(0)d_{xx}(t, 0) = u(t) - n_0\dot{\theta}, \quad (2.2)$$

and a cantilevered beam condition at  $x = 0$ ,

$$d(x, 0) = d_x(t, 0) = 0. \quad (2.3)$$

Two additional boundary conditions state that the shear force and moment at the end of the beam are equal and opposite to the moment and shear force on the mass  $m$ , in which the center of mass of  $m$  is displaced from the beam tip by half of the length of the mass ( $\frac{L_m}{2}$ ),

$$\begin{aligned} \left[ \gamma(x)I(x)\dot{d}_{xx}(t, x) + E(x)I(x)d_{xx}(t, x) \right] \Big|_{x=L} = \\ m \left[ \ddot{d}(t, L) + \frac{L_m}{2}\ddot{d}_x(t, L) + \left(L + \frac{L_m}{2}\right)\ddot{\theta}(t) \right] + f(t), \end{aligned} \quad (2.4)$$

$$\begin{aligned} \left[ \gamma(x)I(x)\dot{d}_{xx}(t, x) + E(x)I(x)d_{xx}(t, x) \right] \Big|_{x=L} = \\ J_1 \left[ \ddot{d}_x(t, L) + \ddot{\theta}(t) \right] - \frac{L_m}{2} \left[ \gamma(x)I(x)\dot{d}_{xx}(t, x) + E(x)I(x)d_{xx}(t, x) \right] \Big|_{x(t,L)}. \end{aligned} \quad (2.5)$$

The disturbance term  $f(t)$  enters the system dynamics through the boundary condition in equation (2.4).

## 2.2 Resulting Finite Element Approximation

A MCS modeled by PDEs is an infinite dimensional system; thus while existence of traditional optimal control schemes can be proven, they cannot be directly implemented [6]. Therefore, the system must be approximated with a sequence of finite dimensional control problems. The finite element method is appropriate for such a system and has been shown to be convergent for this problem [6, 1]. Appendix A contains a detailed derivation of the system of approximating ordinary differential equations (ODEs). The resulting equations that approximate equations (2.1)-(2.5) are

$$\begin{aligned}
 M_s \dot{b} + n_s \dot{\omega} &= -D b - K a \\
 J \dot{\omega} &= q^T a + r^T b + u(t) - n_0 \omega \\
 \dot{a} &= b \\
 \dot{\theta} &= \omega,
 \end{aligned} \tag{2.6}$$

where  $w(t), u(t) \in \mathbf{R}$ , and  $a(t), b(t), n_s, q, r \in \mathbf{R}^{(N)}$ . The above can be represented in matrix form as

$$\begin{bmatrix} I & 0 & 0 & 0 \\ 0 & M_s & 0 & n_s \\ 0 & 0 & 1 & 0 \\ 0 & 0 & 0 & J \end{bmatrix} \begin{bmatrix} \dot{a} \\ \dot{b} \\ \dot{\theta} \\ \dot{\omega} \end{bmatrix} = \begin{bmatrix} 0 & I & 0 & 0 \\ -K & -D & 0 & 0 \\ 0 & 0 & 0 & 1 \\ q^T & r^T & 0 & -n_0 \end{bmatrix} \begin{bmatrix} a \\ b \\ \theta \\ \omega \end{bmatrix} + \begin{bmatrix} 0 \\ 0 \\ 0 \\ 1 \end{bmatrix} u(t) + F_m f(t). \tag{2.7}$$

Let  $z$  be the column vector

$$z = \begin{bmatrix} a \\ b \\ \theta \\ \omega \end{bmatrix}, \quad (2.8)$$

and

$$M_{sys} = \begin{bmatrix} I & 0 & 0 & 0 \\ 0 & M_s & 0 & n_s \\ 0 & 0 & 1 & 0 \\ 0 & 0 & 0 & J \end{bmatrix}, \quad A_{sys} = \begin{bmatrix} 0 & I & 0 & 0 \\ -K & -D & 0 & 0 \\ 0 & 0 & 0 & 1 \\ q^T & r^T & 0 & -n_0 \end{bmatrix}, \quad (2.9)$$

$$B_{sys} = \begin{bmatrix} 0 \\ 0 \\ 0 \\ 1 \end{bmatrix}. \quad (2.10)$$

Equation (2.7) can then be written as

$$\dot{z} = [M_{sys}^{-1} A_{sys}] z + [M_{sys}^{-1} B_{sys}] u(t) + [M_{sys}^{-1} F_m] f(t), \quad (2.11)$$

or, in more compact notation,

$$\dot{z} = Az + Bu(t) + Ff(t) \quad (2.12)$$

$$y = Cz, \quad (2.13)$$

where the matrix  $C$  is determined by the sensed states. This matrix will have a structure equivalent to that in equation (2.14). This structure results from designing the system such that only hub angular position and velocity are sensed.  $C$  will be a  $2 \times (2N + 2)$  matrix where  $N$  is the number of finite element nodes chosen, and has the form

$$C = \begin{bmatrix} \text{zeros}(1, 2N) & 1 & 0 \\ \text{zeros}(1, 2N) & 0 & 1 \end{bmatrix}, \quad (2.14)$$

where the ones appear in the hub position and hub velocity state positions. A  $C$  matrix that corresponds to the sensed state of beam tip velocity, resulting from placement of an accelerometer at the beam tip, would take the form of the following  $3 \times (2N + 2)$  matrix:

$$C = \begin{bmatrix} \text{zeros}(1, N) & \phi(L) & 0 & 0 \\ \text{zeros}(1, 2N) & 1 & 0 \\ \text{zeros}(1, 2N) & 0 & 1 \end{bmatrix}. \quad (2.15)$$

From appendix (A),  $\phi(L) \in \mathbf{R}^N$  is a vector with  $i$ th entry  $\phi_i(L)$ , corresponding to the basis function values at those nodes. Thus, we may write the system as

$$\dot{z} = Az + Bu(t) + Ff(t) \quad (2.16)$$

$$y = Cz \quad (2.17)$$

$$y_{out} = C_{out}z, \quad (2.18)$$

where

$$z = \begin{bmatrix} a & b & \theta & \omega \end{bmatrix}^T, \quad (2.19)$$

and

$$C_{out} = \begin{bmatrix} \text{zeros}(1, 2N) & 1 & 0 \\ \text{zeros}(1, 2N) & 0 & 1 \end{bmatrix}. \quad (2.20)$$

Matrix  $C_{out}$  is the controlled output matrix and returns only the hub angular position and velocity when multiplied by the state vector  $z$ . We choose this output matrix because our only objective is to achieve flapping behavior in the beam using these control schemes. Beam vibration control is secondary and any apparent control is merely a by-product of the coupling of hub and beam dynamics. Again, a complete explanation and derivation of all these terms is found in appendix A.

The form of the system in (2.16) allows for immediate implementation of optimal control. In the next chapter, we solve a general control problem for this system that will be used for both the regulation and tracking problems.

### 3 FLAPPING: AN OPTIMAL CONTROL TRACKING PROBLEM

Linear quadratic control theory was used in this problem rather than ad-hoc methods or PID control schemes because it offers a concept of optimality and has a firm mathematical background, having been used in similar studies such as Gibson and Adamian [3] to great success. Linear quadratic control is a broad term encompassing many control schemes. The specific optimal control schemes used in this work are Linear Quadratic Regulation (LQR), Linear Quadratic Gaussian (LQG), and MINMAX, which is sometimes termed  $\mathcal{H}^\infty$  control.

These control schemes are similar, but LQG and MINMAX control contrast to LQR control in that full state feedback for control is not necessarily assumed. This is a more realistic control scheme since one rarely knows the full state of a system, but rather only a few sensed states. LQG and MINMAX both utilize an optimal estimator, the Kalman-Bucy filter, which rebuilds unknown states from sensed states in a least squares sense. These control schemes are both logical choices for the problem at hand, for while one cannot possibly place sensors along every position of the beam, one could easily sense hub angular position and angular velocity, for example. Perhaps it is also conceivable that an accelerometer be placed on the tip of the beam, such that the velocity of the beam tip could be found by integrating such a signal in real time.

#### 3.1 The Tracking Problem

It is convenient to set the problem up in the form of a tracking problem before we find our optimal control solution. By formulating the problem this way, we can describe the desired system behavior as a mathematical function which our control law can

then drive the system to exhibit. Specifically, flapping behavior can be represented in the form of desired hub position/velocity.

We begin with the model presented at the end of chapter 2.2,

$$\begin{aligned}\dot{z} &= A z + B u(t) + F f(t) \\ y &= C z. \\ z &= C_{out} z.\end{aligned}\tag{3.1}$$

Making the substitution  $x = z - z_d$ , where  $z_d$  is the desired function to track, it is immediately apparent that  $\dot{x} = \dot{z} - \dot{z}_d$ , and so  $\dot{x} + \dot{z}_d = \dot{z}$ . Making these substitutions directly,

$$\begin{aligned}\dot{x} + \dot{z}_d &= A(x + z_d) + B u(t) + F f(t) \\ y &= C x. \\ y_{out} &= C_{out} z.\end{aligned}\tag{3.2}$$

Since the matrix  $A$ , the functions  $z_d$ , and  $\dot{z}_d$  are known, the problem then becomes one of driving the tracking error  $x$  to zero, with the new system of equations written as

$$\begin{aligned}\dot{x} &= A x + B u(t) + F f(t) + (A z_d - \dot{z}_d) \\ y &= C x, \\ y_{out} &= C_{out} z.\end{aligned}\tag{3.3}$$

Our control goal now is to find a general law,  $u(t)$ , using LQG and MINMAX that will induce a flapping motion in the MCS. These approaches can be used for achieving

a variety of goals including: to further enhance the stability of an equilibrium point (motionless beam and zero hub position), to reject a disturbance such as a force upon the tip of the beam, to drive the hub to track a desired function  $z_d \neq 0$  prescribing angular position and velocity, or a combination of these.

### 3.2 A Generalized Control Solution

The control problem can be stated succinctly as the following: Given a known disturbance  $d(t)$ , and an unknown disturbance  $f(t)$ , find the control  $u^*(t)$  and the “worst case disturbance”  $f_d^*(t)$  such that  $(u^*, f_d^*) = \min_u \max_f J(u, f_d)$ , where

$$J = \int_0^{t_f} (x^T Q x + u^T R_1 u - \xi^2 f_d^T R_2 f_d) dt, \quad (3.4)$$

subject to the constraints

$$\dot{x} = Ax + Bu + Ff + d \quad (3.5)$$

$$y = Cx \quad (3.6)$$

$$y_{out} = C_{out}x \quad (3.7)$$

$$d = Az_d - \dot{z}_d \quad (3.8)$$

$$x(0) = z(0) - z_d(0),$$

where

$$C_{out} = \begin{bmatrix} \text{zeros}(1, 2N) & 1 & 0 \\ \text{zeros}(1, 2N) & 0 & 1 \end{bmatrix} \quad (3.9)$$

$$Q = C_{out}^T C_{out} \quad (3.10)$$

$$R_1 = .001 \quad (3.11)$$

$$R_2 = I. \quad (3.12)$$

In general,  $Q$ ,  $R_1$ , and  $R_2$  are weighting matrices. In this work,  $Q$  will be taken simply to be  $C_{out}^T C_{out}$  where  $C_{out}$  is the controlled output matrix (see chapter 2.2).  $R_1$  is a matrix that weights control inputs, but for this problem is a scalar coefficient that weights the input torque on the hub.  $R_2$  is a weighting matrix for the disturbance input to the system (in all cases presented here the identity matrix of proper size).

All of the optimal control schemes previously mentioned can be derived simultaneously, and differ only in terms of a coefficient that weights disturbance knowledge, and state feedback assumptions. This coefficient will be referred to as  $\xi$  (see equation 3.4). When  $\xi = 0$  we obtain LQG control because the disturbance terms are not present in the control cost function and, consequently, are not present in the derivation of the optimal control law solution. One can refer to the following to aid in the understanding of the relationship of these control schemes:

- $\xi = 0$  (No disturbance knowledge in cost function)
  - Full State Feedback
    - \* Linear Quadratic Regulation (LQR)
  - Partial State Feedback (or noisy feedback)
    - \* Linear Quadratic Gaussian (LQG)

- $\xi > 0$  (Weighted disturbance knowledge in cost function)

– Minmax Control and  $\mathcal{H}_\infty$  Methods

The detailed solution to this problem for the LQG case (i.e.  $\xi = 0$ ) can be found in most optimal control textbooks, including [2]. The author was unable to find a general tracking problem solution identical to the one below, and for this reason it is presented. This problem is identical to the general problems solved in textbooks, but for the MINMAX case (i.e.  $\xi > 0$ ), extra terms involving  $\xi$  are found in the solution to the tracking problem.

The optimal solution  $(u^*, \xi^*)$  is a saddle point of the cost functional. If  $(x, u, \xi)$  satisfies the differential equations, then

$$J = \int_0^{t_f} (x^T Q x + u^T R_1 u - \xi^2 f(t)^T R_2 f(t) + \lambda^T (Ax + Bu + F f(t) + d - \dot{x})) dt,$$

which can be rewritten as

$$\begin{aligned} J = & -\lambda^T(t_f)x(t_f) - \lambda^T(t_f)d(t_f) + \lambda^T(0)d(0) + \lambda^T(0)x(0) \\ & + \int_0^{t_f} H(x, u, f(t), \lambda) + \lambda^T \dot{x} dt, \end{aligned} \quad (3.13)$$

where

$$H = x^T Q x + u^T R_1 u - \xi^2 f(t)^T R_2 f(t) + \lambda^T (Ax + Bu + F f(t) + d) dt. \quad (3.14)$$

From calculus of variations, the necessary conditions for optimizers (saddle point) are

$$\begin{aligned}
 \frac{\partial H}{\partial u} &= 0 \\
 \frac{\partial H}{\partial w} &= 0 \\
 \dot{\lambda} &= -\left(\frac{\partial H}{\partial x}\right)^T \\
 \lambda(t_f) &= 0.
 \end{aligned} \tag{3.15}$$

Differentiating  $H(x, u, f(t), \lambda)$  with respect to  $u$  and solving for  $u$  yields

$$u = -\frac{1}{2}R_1^{-1}B^T\lambda. \tag{3.16}$$

Repeating the process for  $w$  yields

$$w = -\frac{\xi^2}{2}R_2^{-1}D^T\lambda. \tag{3.17}$$

Now

$$\begin{aligned}
 \dot{\lambda} &= -\left(\frac{\partial H}{\partial x}\right)^T \\
 &= -(2x^TQ + \lambda^T A)^T \\
 &= -2Q^T x - A^T \lambda.
 \end{aligned} \tag{3.18}$$

We proceed with the assumption that  $\lambda = 2\Pi x + 2b$ , where  $b$  will be a feed forward function to be found later. We choose this form because of experience and similarities to the LQG and LQR derivations. Differentiating  $\lambda$  with respect to time,

$$\dot{\lambda} = 2\dot{\Pi}x + 2\Pi\dot{x} + 2\dot{b}, \tag{3.19}$$

equation (3.18) becomes

$$\dot{\lambda} = -2Q^T x - 2A^T \Pi x - 2A^T b. \quad (3.20)$$

Substituting  $\dot{x} = Ax + Bu + Df(t) + d$  into equation (3.20) yields

$$\dot{\lambda} = 2\dot{\Pi}x + 2\Pi Ax + 2\Pi Bu + 2\Pi Ff + 2\Pi d + 2\dot{b}. \quad (3.21)$$

Replacing  $\lambda$  in equations (3.16) and (3.17) with the assumption  $\lambda = 2\Pi x + 2b$  and simplifying yields

$$u = -R_1^{-1} B^T \Pi x - R_1^{-1} B^T b \quad (3.22)$$

$$w = -\xi^2 R_2^{-1} D^T \Pi x - \xi^2 R_2^{-1} D^T b. \quad (3.23)$$

Substituting  $u$  and  $w$  into equation (3.21) and comparing coefficients of  $x$ ,  $b$ ,  $\dot{b}$ , and  $d$  yields the MINMAX Differential Ricatti Equation (MMDRE), and a differential equation for  $b$ ,

$$-\dot{\Pi} = \Pi A + A^T \Pi - \Pi B R_1^{-1} B^T \Pi + \xi^2 \Pi F R^{-1} F^T \Pi + Q \quad (3.24)$$

$$\dot{b} = -(A^T + \xi^2 \Pi F R^{-1} D^T - \Pi B R^{-1} B^T) b - \Pi d. \quad (3.25)$$

Equation (3.24) is the general solution for  $\Pi(t)$ . Setting  $\dot{\Pi} = 0$  yields the *steady state regulator* problem, in which the optimization time interval is infinite. This process yields the algebraic Ricatti equation (ARE),

$$0 = \bar{\Pi} A + A^T \bar{\Pi} - \bar{\Pi} B R_1^{-1} B^T \bar{\Pi} + \xi^2 \bar{\Pi} D R^{-1} F^T \bar{\Pi} + Q, \quad (3.26)$$

where  $\bar{\Pi}$  denotes the steady state solution for  $\Pi(t)$ . Thus the control problem for the finite element system is written

$$\begin{aligned}\dot{x}(t) &= Ax(t) + Bu(t) + Ff(t) + d(t) \\ y(t) &= Cx(t) \\ d(t) &= Az_d(t) - \dot{z}_d(t) \\ u(t) &= -R_1^{-1}B^T\bar{\Pi}x(t) - R_1^{-1}B^Tb(t),\end{aligned}$$

where  $b(t)$  is the solution to equation (3.25).

This system assumes full state feedback, which is not the case in this study. We therefore introduce the concept of the LQG and MINMAX compensator. The theory behind the following mathematics can be found in [2].

Let  $x_c$  denote the estimated states found by application of the filter Ricatti equation solution  $P$ . The complete system, which does not assume full state feedback and can estimate the system states from limited sensor output, is

$$\begin{aligned}\dot{x}(t) &= Ax(t) + Bu + Ff(t) + d(t) \\ \dot{x}_c(t) &= Ax_c(t) + Bu - PCx_c(t) + Py(t) + d(t) \\ y(t) &= Cx \\ y_{out} &= C_{out}x_c \\ d(t) &= Az_d(t) - \dot{z}_d(t) \\ u(t) &= -R_1^{-1}B^T\bar{\Pi}x(t) - R_1^{-1}B^Tb(t).\end{aligned}$$

This system of equations can now be used to simulate a system driven to exhibit flapping behavior using optimal control with only partial state feedback. For instance,

choosing  $z_d(t) = \theta_d(t) = \sin(t)$  would yield a system in which the hub actuator is driven to a periodic motion in  $\theta$ , which results in a “flapping” beam as a bi-product of this desired hub angle. A variation of this proposed simulation is presented in the next chapter.

## 4 SIMULATIONS AND RESULTS

This chapter introduces the problems and respective simulation results. Four distinct problems will be stated and solved (see list below).

- Uncontrolled System ( $u(t) = 0$ )
- Regulation with Tip Force Disturbance
- Tracking (Flapping)
  - No Disturbance
  - Tip Force Disturbance

The uncontrolled case will act as a basis for comparison as to the effect a tip force can have upon the system, as well as the noticeably different result that occurs when optimal control is introduced. A brief comparison between an aluminum beam and a bone beam will be made to emphasize how the difference in rigidity results in different behavior as expected. The regulation (stabilization) problem will demonstrate the success of LQG and MINMAX at rejecting unknown disturbances. The tracking simulations section will demonstrate the effectiveness of LQG and MINMAX when tracking a desired function (described below).

Functions chosen to describe varying parameters are considered an approximation to bat bone physiology scaled to the size of micro air vehicles (wing length on the order of 30 centimeters).

The chosen beam density is a crude approximation to real bat bone density. It was found by treating the bones as perfectly cylindrical and simply finding the ratio of mass to volume. The density found for the longest bone in the bat wing was used so that the cylindrical measurement error was minimized. The density used,  $1450 \text{ kg/m}^3$ , is stated in Table 4.1 along with the other beam parameter values.

Table 4.1: Beam Parameters

	$\rho$ ( $kg/m^3$ )	$E$ ( $Nm^2$ )	$\gamma$ ( $Ns/m^2$ )	<i>Width/Thick@Hub</i> ( $cm$ )	<i>@Tip</i> ( $cm$ )
<i>Aluminum</i>	2700	$7.0 \times 10^{10}$	$1.219 \times 10^6$	1.0	.5
<i>Bone</i>	1450	$2.3 \times 10^{10}$	$1.219 \times 10^7$	1.0	.5

## 4.1 Model Problems

This section introduces four model problems used to evaluate and compare several control schemes using these varying bone-like parameters. Each problem either introduces a disturbance similar to that of a gust of wind (force on the tip) and/or tracking a function, in order to show how a controller would react to a real disturbance of force on such a system. Both the simple regulation scenario and the more complicated tracking scenario, in which it is desired that the hub/beam system exhibit a certain behavior, are exposed to varying disturbances.

An example of a gust profile is shown in Figure 4.1. Choosing this function,  $f(t) = 10 e^{-2(t-4)^2}$ , while seemingly arbitrary, is nonetheless appealing to intuition as to what the force from a gust of wind might look like. The force is negligible except for a period of approximately two seconds, during which it quickly rises and falls to a maximum magnitude of ten Newtons.

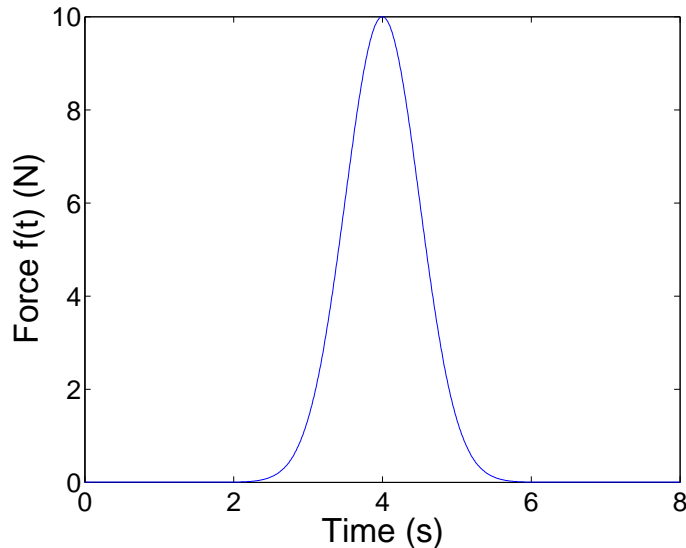


Figure 4.1: Tip force profile

## 4.2 Uncontrolled without a Disturbance

To illustrate the difference in deflection between aluminum and a bone-like material, we chose the initial deflection to be the first mode of a beam with a constant cross sectional area (taken directly from [4]).

$$d_0(x) = \frac{1}{2}(\cosh\beta_n x - \cos\beta_n x - \sigma_n(\sinh\beta_n x - \sin\beta_n x)) \quad (4.1)$$

where  $\sigma_n = 0.7341$  and  $\beta_n = 1.87510407/L$ . This initial deflection allows for beam deflection and vibrations to be evident. The initial hub displacement,  $\theta(0) = 0$ , hub velocity,  $\omega(0) = 0.1$ , and forcing,  $f(t) = 0$ , are chosen so that the first uncontrolled problem exhibits variations in hub position due to beam vibrational feedback. Parameters for each beam are shown in Table 4.1. The initial hub angular velocity was chosen to be 0.1 rad/s in this problem to fully introduce the physics of the system. Thus there will be beam vibrations and hub velocity present with no control input,

just damping in the system.

The tapering of the beam along with the low Young's modulus and density contribute to increased flexibility. The tip deflection of each is shown below in Figures 4.2(a) - 4.2(b).

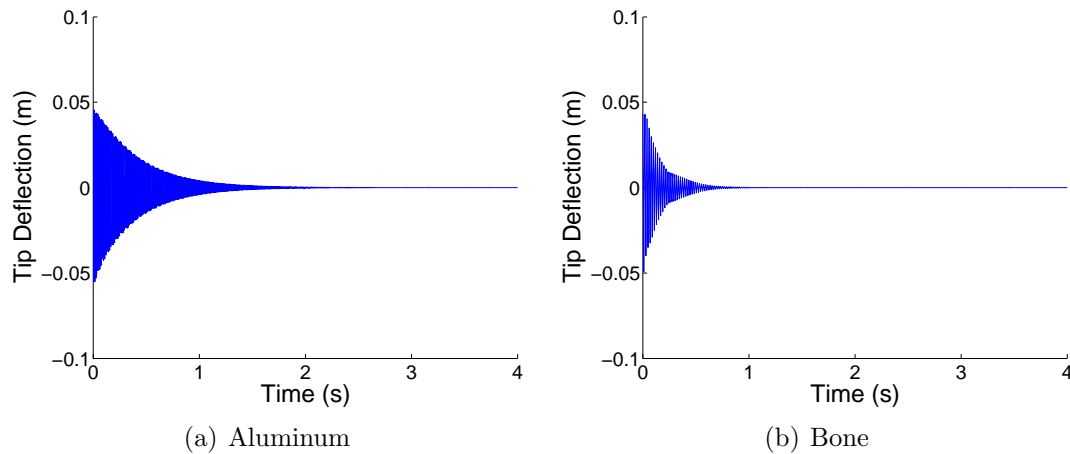


Figure 4.2: Uncontrolled beam tip deflection

As expected, the bone beam oscillates slower than the aluminum beam. Also, the bone dynamics are damped quicker by the larger Kelvin-Voigt damping constant (see Table 4.1).

The system can rotate fully about the hub as will be made apparent in the next section. Figures 4.3(a) - 4.3(b) represent that angle.

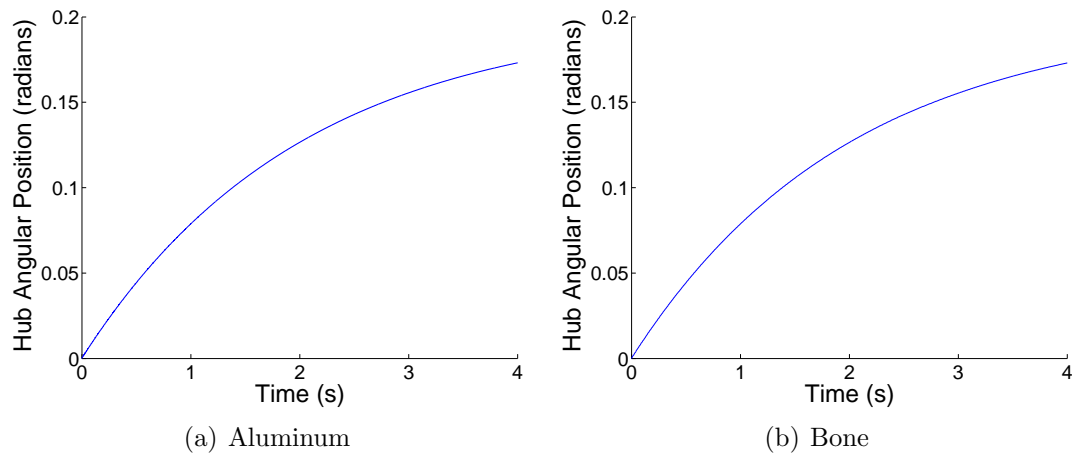


Figure 4.3: Uncontrolled hub angular position

Note in Figures 4.3(a) - 4.3(b) the position is asymptotically approaching some value; this is consistent with the initial hub position and velocity with damping present. Also associated with the hub is rotational velocity, displayed in Figures 4.4(a) - 4.4(b). In this problem, the initial angular velocity was 0.1 rad/s. The hub friction is readily apparent due to the decrease in hub rotational velocity.

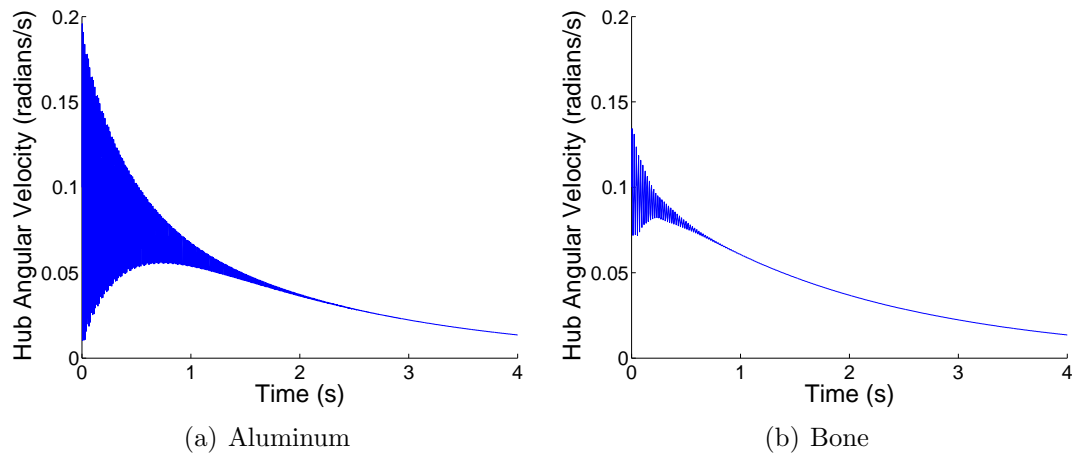


Figure 4.4: Uncontrolled hub angular velocity

Figures 4.5(b)-4.5(a) are surface plots of the system. The beam position is rotated to incorporate hub position. The circles on each end represent the bounds of beam

rotation and aid with visualization. The hub position is represented as a thick line in the center from which the beam extends. The tip mass is not present in the image.

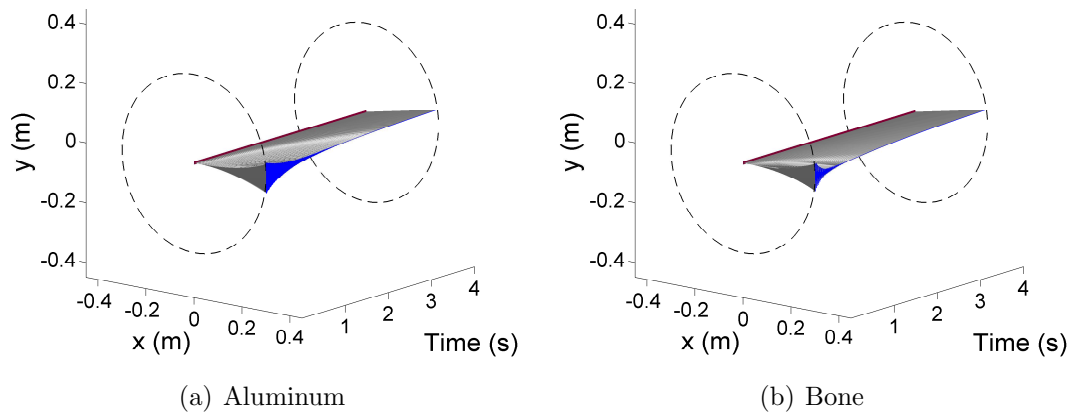


Figure 4.5: Uncontrolled system surface plot

In these simulations, no tip force disturbance was present. The next section demonstrates the effect of such a force on the system.

### 4.3 Uncontrolled in the Presence of a Disturbance

In the previous simulation, there was no force acting on the beam tip. To demonstrate the result of a gust force upon the tip mass of an uncontrolled system we use the disturbance

$$f(t) = 10e^{-2(t-4)^2}.$$

For an uncontrolled beam we would intuitively expect a force on the tip to bend the beam due to the shear force, causing an increasing hub angular velocity during the force duration. This velocity decreases afterwards due to hub friction and beam damping.

The tip deflection remains unchanged except for the effect of the force on the tip, which bends the beam during a small time interval.

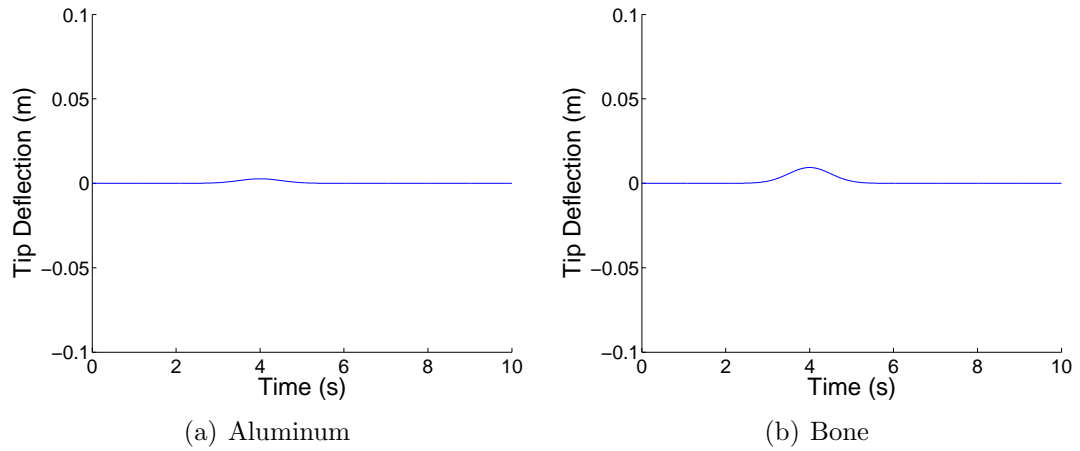


Figure 4.6: Uncontrolled/disturbed: Tip deflection

Both the hub velocity and position increase due to the force, with hub velocity decreasing due to hub friction. These result in the hub eventually approaching a final position.

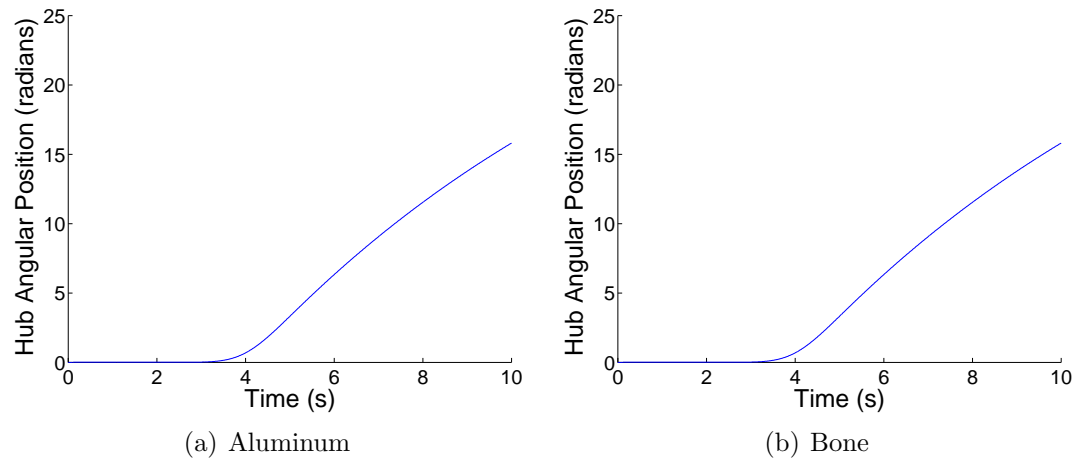


Figure 4.7: Uncontrolled/disturbed: Hub angular position

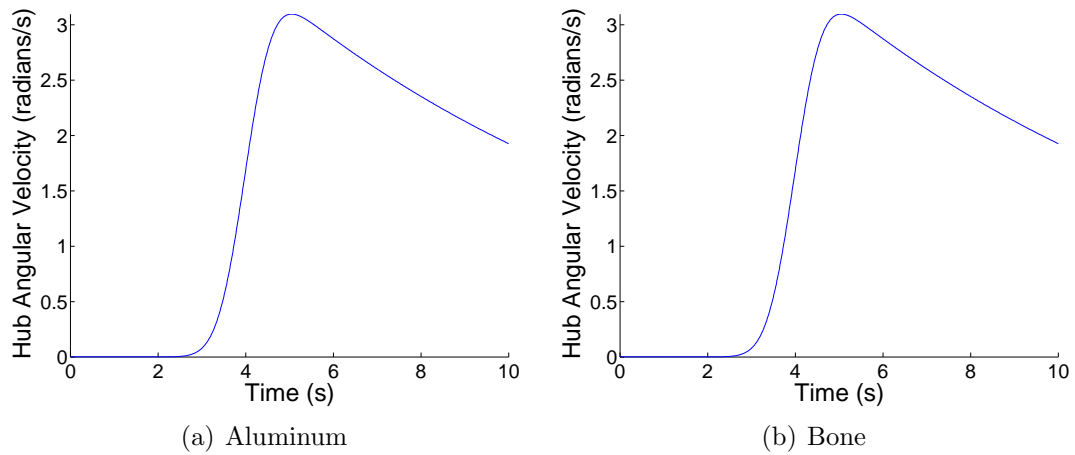


Figure 4.8: Uncontrolled/disturbed: Hub angular velocity

The effect of a tip force upon the system is best visualized with the following surface plot (Figure 4.5(b)). The result is a spinning hub and beam, only slowed by friction.

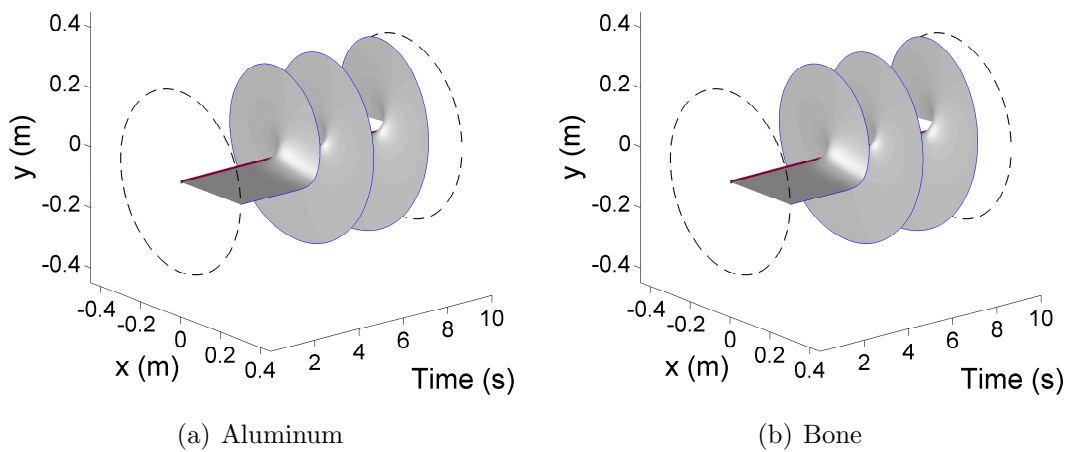


Figure 4.9: Uncontrolled/disturbed: Surface plot

The above simulation demonstrates the success (at least intuitively) of the model. In the next section, a control torque at the hub is used to attenuate the beam rotation

observed in the uncontrolled case. From this point on, we will drop the aluminum beam counterpart and focus solely upon controlling the more flexible bone beam.

It is also apparent from the above that there is little difference between an aluminum beam and bone beam at this scale in terms of reaction to disturbances like the one chosen here. The only obvious difference is in the frequency of beam vibrations (Young's modulus and Kelvin-Voigt constant) and overall weight of the system.

#### 4.4 Regulation in the Presence of a Disturbance

The previous simulation demonstrated what a gust force disturbance can do to such a system. In the following, we include the effects of a disturbance force on the beam tip centered at time  $t = 4$ , but with a control input at the hub.

First, note the tip deflection in Figure (4.10). At four seconds the beam experiences a tip forcing like that shown in Figure (4.1). Like the uncontrolled case in section 4.3, the system begins to rotate.

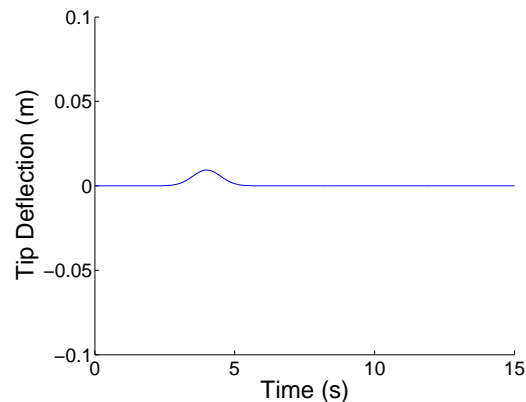


Figure 4.10: Controlled/disturbed: Tip deflection

The following panel of figures (Figures 4.11(a)-4.11(c)) illustrates the differences between the control schemes in terms of applied control. Notice the similarities be-

tween LQR and LQG.

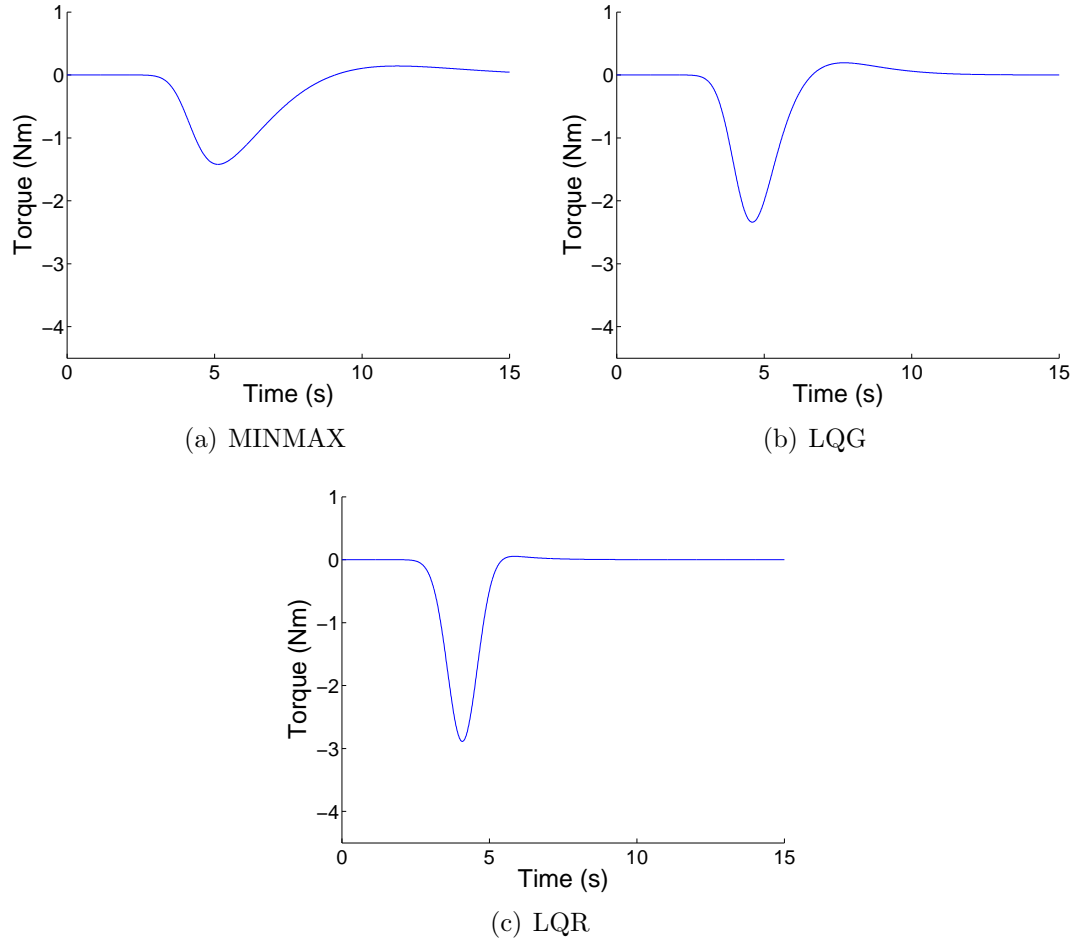


Figure 4.11: Controlled/disturbed: Control exerted by hub

Note that LQR applied more torque than the other schemes, for the same control parameter set. The most important difference is the time at which LQR applied this force. It is almost immediately after the gusting force is exerted on the tip. MINMAX and LQG both lag a little in applying control. This difference may be due to the partial state feedback of MINMAX and LQG versus the full state feedback of LQR.

Surface plots of each simulation are shown below in Figures 4.12(a)-4.12(c). No-

tice the substantial differences between each in terms of recovery time and overall disturbance effect. LQG does substantially better than MINMAX in terms of total angular position; the latter rotating over  $\pi/2$  radians further from the zero position.

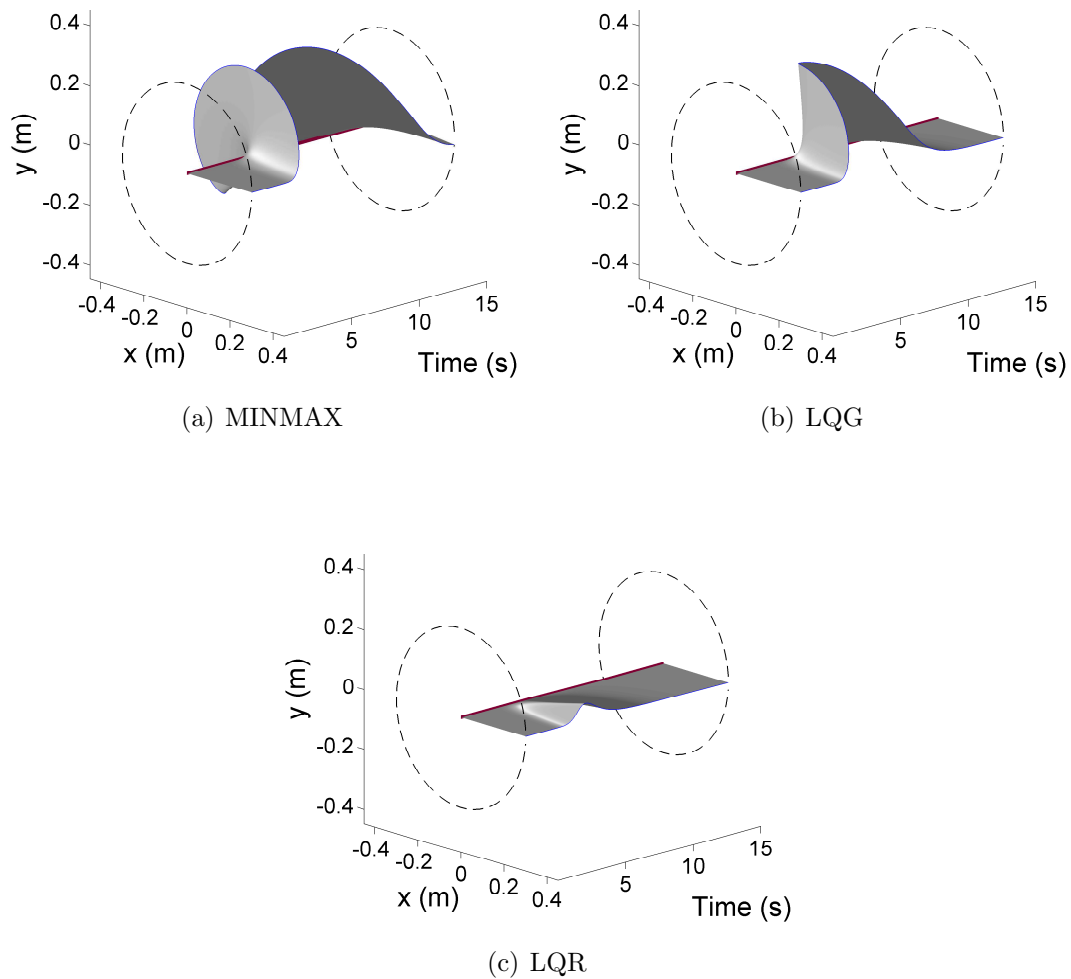


Figure 4.12: Uncontrolled/disturbed: Hub angular position/velocity

All the control schemes drive the system back to the desired position ( $\theta = 0$ ), MINMAX (henceforth referred to as MM) takes several seconds longer to reject this disturbance. We hypothesize that one reason MM is less successful than LQG is the way the disturbance enters the control derivation. The MM control law is built using

the force matrix  $F$  (see appendix A), limiting the knowledge of the disturbance solely to the effect such a disturbance would have upon the tip of the beam. It was not investigated how to overcome this limitation.

## 4.5 Tracking without a Disturbance

Flapping behavior can be considered a tracking problem. In a system designed for flapping flight, it is probably desired that the wing follow a specified trajectory and with a given frequency. In this section, we change our desired function for hub angular position  $\theta(t)$  from zero to a specified periodic function  $\theta_d(t)$  that describes the desired hub angle  $\theta_d(t)$ . We then solve the control problems in the same way we did for the regulation case.

Henceforth LQR will be omitted in the results shown in this section. The solution to the LQR problem is not of interest since it relies on unrealistic assumptions. The corresponding LQR simulations can still be found in appendix B for each respective problem.

The control solution to the tracking problem is represented in Figures 4.13(a)-4.13(b) as the torque applied at the hub.

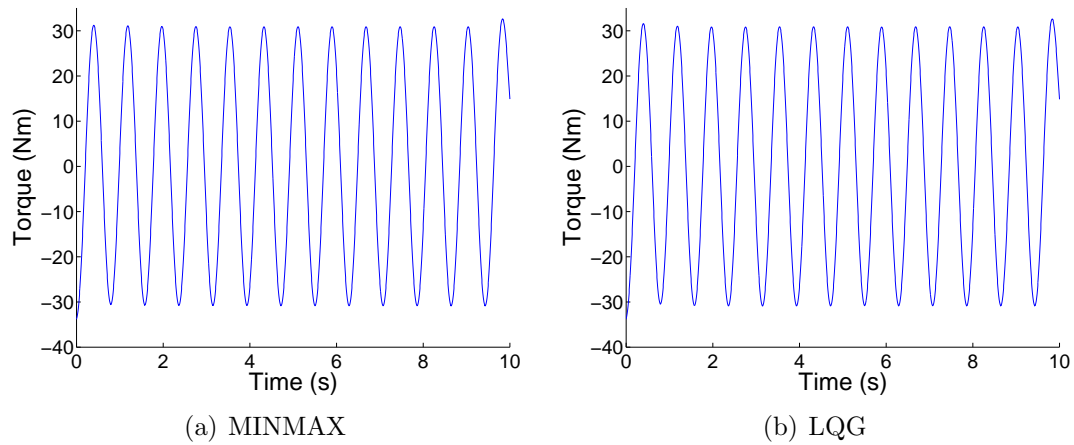


Figure 4.13: Tracking: Control torque

The control in the figures above drives the system to exhibit the behavior shown in Figures 4.14(a)-4.16(b). Notice the discrepancy between the actual and desired hub positions in this set of figures. This is an artifact of limiting the available torque on the system by heavily weighting the terms involving control in the cost function (see matrix  $R_1$  in Equation (3.4)).

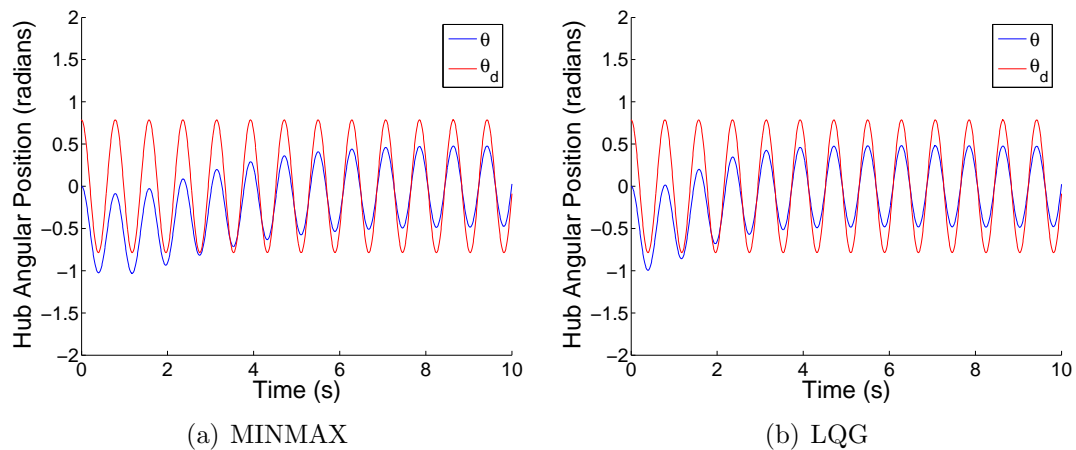


Figure 4.14: Tracking: Hub angular position

This could be improved by allowing for more control in the cost function (see  $R_1$  matrix in equation (3.4)) as shown briefly in Figures 4.15(a) and 4.15(b), in which

$R_1 = 0.001$  versus  $R_1 = 0.01$  in all other simulations. We will retain the less powerful control as a standard.

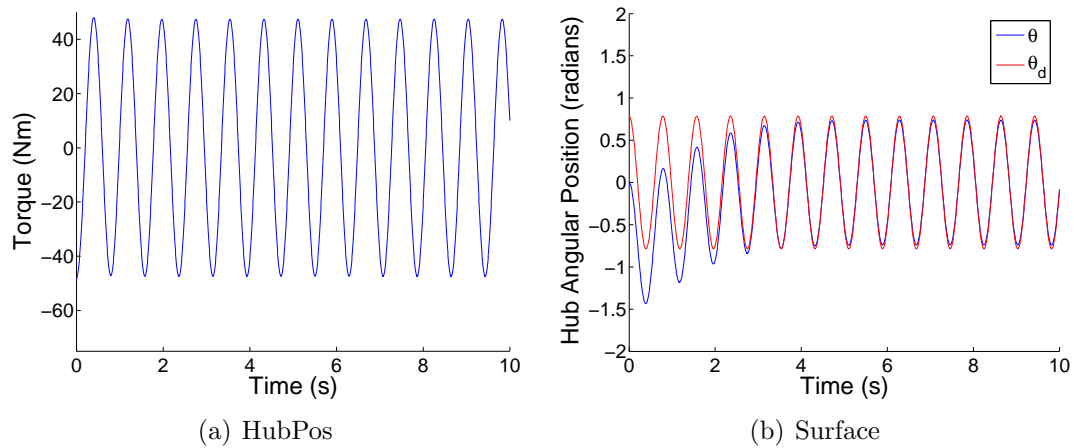


Figure 4.15: Tracking: Hub position tracking with greater control

This control shown in Figure 4.13(a) and 4.13(b) drives the system to exhibit the overall behavior shown in Figures 4.16(a) - 4.16(b).

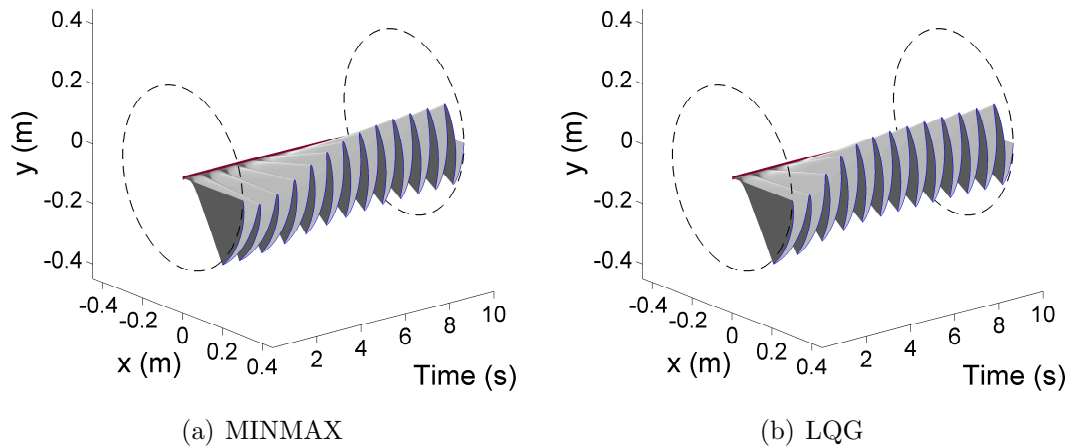


Figure 4.16: Tracking: System surface plot

The next section will introduce a disturbance and compare the control schemes in their ability to reject a gusting force on the wing tip.

## 4.6 Tracking in the Presence of a Disturbance

Subjecting the flapping hub/beam system to a tip force disturbance identical to that in subsection 4.4, we notice a similar difference between MM and LQG in rejecting the disturbance, with LQG performing better again. In Figure 4.17(a), MM takes several seconds longer than LQG to correct the rotation caused by the disturbance.

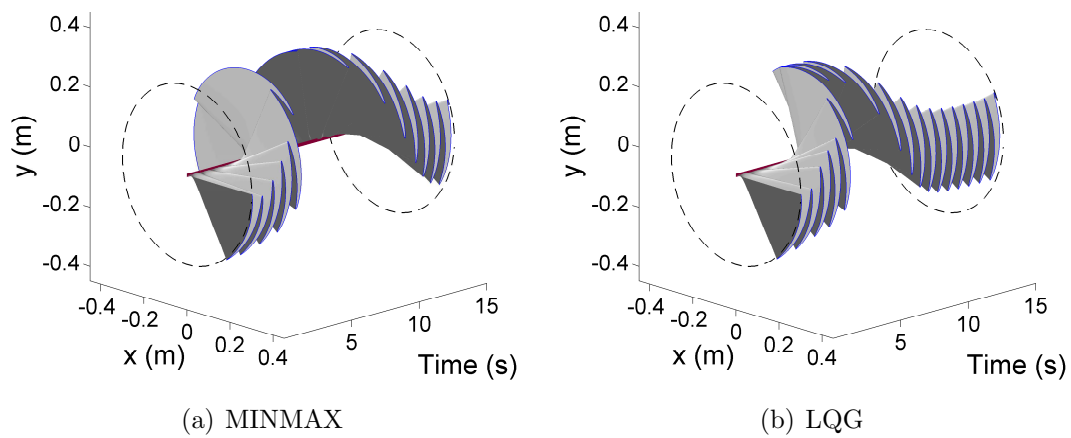


Figure 4.17: Tracking/disturbed: System surface plot

This system response is associated with the control inputs shown in Figures 4.18(a) and 4.18(b) below.

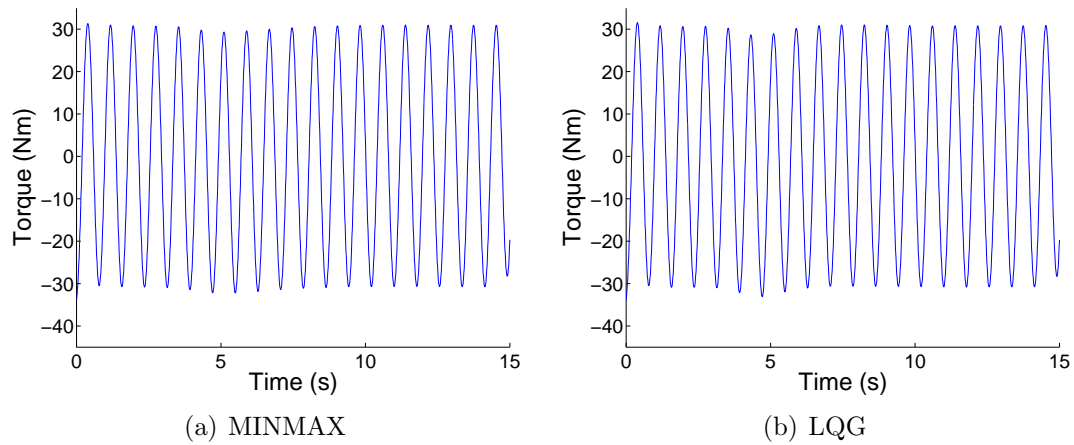


Figure 4.18: Tracking/disturbed: Control

Why does MM not perform as well as LQG? This question may be answered intuitively by considering the structure of the mathematical system in equation set (3.27). While the hub is fully capable of attenuating beam harmonics, as is investigated in [5], we have chosen a sensor output matrix  $C$  that does not grant us direct access to those states, since some beam vibrations are attenuated due to their direct influence upon the hub position. This association contrasts to the disturbance matrix  $F$  introduced in chapter 2.2, which is only directly associated with the tip of the beam.

## 5 CONCLUSIONS

In this study, we investigated the use of optimal control theory to achieve a periodic flapping behavior in a multiple component structure consisting of a rotating hub actuator, a flexible beam, and a prescribed tip mass. More specifically, we achieved this desired behavior by solving an optimal tracking problem. Both LQG and MM control theories were used to achieve the behavior, and a comparison and contrast of the implementation and performance of each was discussed.

We solved four model problems, beginning with the uncontrolled case. We saw that when the system experiences a disturbance, such as a force upon the tip, the hub and beam are sent into a spiralling behavior that is only slowed by friction in the hub and beam material damping.

In the next model problem, we studied regulation. This was a problem in which we wished to drive the system to zero state conditions. We introduced a disturbance on the tip, and unlike the uncontrolled case which spiraled out of control, the system was driven back to the zero position by the hub actuator, and the beam vibrations were also eliminated in less time than they would have with material damping only.

For the final two problems, we solved the tracking problem necessary to drive the system to flapping behavior. We first defined flapping behavior as a periodic function at the hub, which causes the beam to follow a path that traces out a circular arc with a specified angle - a flapping behavior that appeals to intuition. Both MM and LQG were successful in achieving this behavior. With the introduction of a disturbance however, MM took substantially longer to regain control. Of course, with a much deeper investigation into tuning the parameters used in the computing of the control law, we may find a better control scheme. The knowledge gained here is that, while MM delivers robustness against a disturbance up to a certain threshold,

LQG performs better even though it is entirely ignorant of the disturbance and the way it can enter the system dynamics.

Exploring the structure of the system may offer an explanation as to why MM performed worse. The structure of the disturbance matrix  $F$  in the system equations effectively disconnects the disturbance from the hub. The disturbance affects the entire system through the coupled nature of the finite element components, and is therefore still physically realistic. The issue is that, in the computation of the MM controller, the disturbance matrix is completely different from the input matrix  $B$ . Thus, the worst case disturbance that MM is capable of rejecting has little to do with the disturbance in hub rotation. In fact, the presence of the disturbance terms in the MM system are having a detrimental effect on the feed-forward tracking terms. These ideas, and the fact that LQG performs comparably well to the optimal LQR controller, lead us to conclude that while LQG has no robustness margins, it will nonetheless be a better choice than MM and may be capable of performing in such a flapping system.

For the problem of designing a flapping system, a control scheme that is simple, computationally fast, and can estimate the system states through very few measurements will likely be the best candidate. Both LQG and MM optimal control schemes are likely candidates for a system that balances design and controlled behavior, and one that will exhibit robustness against gusting wind conditions. The ease of implementation and performance of LQG presented here leads us to conclude that it is the best choice. The fact that it required only two sensed states corresponding to the hub is an indication of a good choice for an estimation and control scheme for this system.

Of course this is only the beginning in designing such a system. Future work should include building the hub/beam system and studying the performance of con-

trol schemes again. A more complete look into the nature of flapping flight is also necessary for this investigation. Future work could also include the addition of more complicated structures such as coupled flexible beams and/or flexible membranes such as that found in bats. The question of how to model these structures effectively is one of great importance and interest. These are just a few of the many possible areas for future work.

## BIBLIOGRAPHY

- [1] J. Burns, D. Inman, E. Ruggiero, and J. Singler. Finite element formulation for static shape control of a thin euler-bernoulli beam using piezoelectric actuators. *Proceedings of the 2004 ASME International Mechanical Engineering Conference and Exhibition*, pp. 9-16, 2004.
- [2] P. Dorato, C.T. Abdallah, and V. Cerone. *Linear quadratic control: An introduction*. Prentice-Hall, Inc., 1995.
- [3] J.S. Gibson and A. Adamian. Approximation theory for linear-quadratic-gaussian optimal control of flexible structures. *SIAM Journal on Control and Optimization*, 29:1–37, 1991.
- [4] D.J. Inman. *Engineering vibration*. Prentice-Hall, Inc., 1994.
- [5] B.B. King. *Modeling and control of multiple component structures*. PhD thesis, Clemson University, 1991.
- [6] B.B. King. Modeling and control of a multiple component structure. *Journal of Mathematical Systems, Estimation and Control*, 4:1–36, 1994.
- [7] T.H. Kunz, U.M. Norberg, J.F. Steffensen, O. Von Helversen, and Y. Winter. The cost of hovering and forward flight in a nectar-feeding bat, *glossophaga soricina*, estimated from aerodynamic theory. *Journal of Experimental Biology*, 182:207–227, 1993.
- [8] T.H. Kunz, H.M. Papadimitrion, and S.M. Swartz. Ontogenetic and anatomic variation in mineralization of the wing skeleton of the mexican free-tailed bat, *tadarida brasiliensis*. *Journal of Zoology*, 240:411–426, 1996.
- [9] K.M. Middleton and S.M. Swartz. Biomechanics of the bat limb skeleton: Scaling, material properties, and mechanics. *Cells Tissues Organs*, 187:59–84, 2007.
- [10] S. Swartz, M. Bennet, and D.R. Carrier. Wing bone stresses in free flying bats and the evolution of skeletal design for flight. *Nature*, 359:726–729, 1992.
- [11] Sharon Swartz. Skin and bones: the mechanical properties of bat wing tissues. In *Bats: Phylogeny, Morphology, Echolocation, and Conservation Biology*, pages 109–126. Smithsonian Inst. Press, 1998.
- [12] S.M. Swartz. Allometric patterning in the limb skeleton of bats: Implications for the mechanics and energetics of powered flight. *Journal of Morphology*, 234:277–294, 1997.
- [13] S.M. Swartz, M.S. Groves, H.D. Kim, and W.R. Walsh. Mechanical properties of bat wing membrane skin. *Journal of Zoology*, 239:357–378, 1996.

- [14] S.M. Swartz, J. Iriarte-Diaz, D.K. Riskin, A. Song, X. Tian, D.J. Willis, and K.S. Breuer. Wing structure and the aerodynamic basis of flight in bats. *American Institute of Aeronautics and Astronautics Journal*, 42:1–10, 2007.
- [15] C. Voigt and Y. Winter. Energetic cost of hovering flight in nectar-feeding bats and its scaling in moths, birds, and bats. *Journal of Comparative Physiology B-Biochemical System and Environmental Physiology*, 169(1):38–48, 1999.
- [16] P. Watts, E.J. Mitchell, and S. Swartz. A computational model for estimating the mechanics of horizontal flapping flight in bats: Model description and validation. *Journal of Experimental biology*, 204(16):2873–2898, 2001.
- [17] T. Xiaodong, J. Iriarte-Diaz, K. Middleton, R. Galvao, E. Israeli, A. Roemer, A. Sullivan, A. Song, S. Swartz, and K. Breuer. Direct measurements of the kinematics and dynamics of bat flight. *Proceedings of 36th AIAA Fluid Dynamics Conference*, 1:S10-S18, 2006.

APPENDICES

## A FINITE ELEMENT DERIVATION

In this portion of the appendix, we present the finite element method used to approximate the solution to the PDE in equation (2.1). We use cubic B-splines for basis functions. Also, for compactness, we rewrite individual parameters as combined functions varying in  $x$ , and drop dependence on  $x$  and  $t$  when unambiguous. For example, in equation (2.1),  $\rho(x)A(x)$  is rewritten as  $\rho A(x)$ , which will be further simplified as  $\rho A$ . It is assumed throughout this derivation that all parameters may vary in  $x$ , so that no loss of generality occurs.

We begin by finding the *weak form* of the equations by multiplying equation (2.1) by test function  $\phi = \phi(x)$  and integrating from  $x = 0$  to  $x = L$ ,

$$\int_0^L (\rho A)[\ddot{d} + x\ddot{\theta}] \phi \, dx + \int_0^L (\gamma I \dot{d}_{xx} + E I d_{xx})_{xx} \phi \, dx = 0. \quad (\text{A.1})$$

We must balance the spatial derivatives of the unknowns and the test function  $\phi(x)$  by integrating equation (A.1) by parts twice in the second integral,

$$\int_0^L (\rho A) [\dot{d} + x\dot{\theta}] \phi \, dx + \int_0^L (\gamma I \dot{d}_{xx} + E I d_{xx}) \phi_{xx} \, dx + \left( \left[ \gamma I \dot{d}_{xx} + E I d_{xx} \right]_x \phi - \left[ \gamma I \dot{d}_{xx} + E I d_{xx} \right] \phi_x \right) \Big|_0^L = 0. \quad (\text{A.2})$$

This introduces additive boundary terms, which can be simplified by choosing  $\phi(0) = 0$  and  $\phi_x(0) = 0$ , eliminating the terms evaluated at  $x = 0$  and guaranteeing the test functions satisfy the geometric boundary conditions. Therefore, the *weak form*

of equation (2.1) is

$$\int_0^L (\rho A) \left[ \dot{d} + x\ddot{\theta} \right] \phi dx + \int_0^L (\gamma I \dot{d}_{xx} + E I d_{xx}) \phi_{xx} dx + \left( \left[ \gamma I \dot{d}_{xx} + E I d_{xx} \right]_x \phi - \left[ \gamma I \dot{d}_{xx} + E I d_{xx} \right] \phi_x \right) \Big|_{x=L} = 0. \quad (\text{A.3})$$

The boundary condition terms can then be further simplified using equations (2.4-2.5) and made to include the tip mass and disturbance tip force dynamics. Recall equation (2.5),

$$\left[ \gamma(x)I(x)\dot{d}_{xx}(t, x) + E(x)I(x)d_{xx}(t, x) \right] \Big|_{x=L} = J_1 \left[ \ddot{d}_x(t, L) + \ddot{\theta}(t) \right] - \frac{L_m}{2} \left[ \gamma(x)I(x)\dot{d}_{xx}(t, x) + E(x)I(x)d_{xx}(t, x) \right]_x \Big|_{(t,L)}. \quad (\text{A.4})$$

From equation (2.4),

$$\left[ \gamma(x)I(x)\dot{d}_{xx}(t, x) + E(x)I(x)d_{xx}(t, x) \right]_x \Big|_{x=L} = m \left[ \ddot{d}(t, L) + \frac{L_m}{2} \ddot{d}_x(t, L) + \left( L + \frac{L_m}{2} \right) \ddot{\theta}(t) \right] + f(t). \quad (\text{A.5})$$

Substituting equation (A.5) into equation (A.4) and rearranging, we obtain

$$\left[ \gamma(x)I(x)\ddot{d}_{xx}(t, x) + E(x)I(x)d_{xx}(t, x) \right]_x \Big|_{x=L} = \frac{L_m}{2} \left( m \left[ \ddot{d}(t, L) + \frac{L_m}{2} \ddot{d}_x(t, L) + \left( L + \frac{L_m}{2} \right) \ddot{\theta}(t) \right] + f(t) \right) - J_1 (\ddot{d}_x + \ddot{\theta}) - \frac{L_m}{2} f(t). \quad (\text{A.6})$$

After substituting these terms back into equation (A.3), we find the simplified *weak*

form of the system equations is the set of second order equations

$$\begin{aligned}
& \int_0^L (\rho A) [\dot{d} + x\ddot{\theta}] \phi dx + \int_0^L (\gamma I \dot{d}_{xx} + E I d_{xx}) \phi_{xx} dx \\
& + \left( m \left[ \ddot{d}(t, L) + \frac{L_m}{2} \ddot{d}_x(t, L) + \left( L + \frac{L_m}{2} \right) \ddot{\theta}(t) \right] + f(t) \right) \phi(L) \\
& - \frac{L_m}{2} \left( m \left[ \ddot{d}(t, L) + \frac{L_m}{2} \ddot{d}_x(t, L) + \left( L + \frac{L_m}{2} \right) \ddot{\theta} \right] + f(t) \right) \phi_x(L) \\
& + J_1 (\ddot{d}_x + \ddot{\theta}) \phi_x(L) - \frac{L_m}{2} f(t) \phi_x(L) = 0, \tag{A.7}
\end{aligned}$$

and

$$J_0 \ddot{\theta}(t) - \gamma I(0) \dot{d}_{xx}(t, 0) - E I(0) d_{xx}(t, 0) = u(t) - n_0 \dot{\theta}. \tag{A.8}$$

To build the finite element system of ordinary differential equations, convert the above equations to first order form (i.e. let  $v(t, x) = \dot{d}(t, x)$  and  $\omega(t) = \dot{\theta}(t)$ ). Rearranging, we arrive at the weak form for the combined beam/hub system of equations which includes the beam/hub interaction equation,

$$\begin{aligned}
& \int_0^L (\rho A) [v + x\dot{\omega}] \phi dx + \int_0^L (\gamma I v_{xx} + E I d_{xx}) \phi_{xx} dx \\
& + \left( m \left[ \dot{v}(t, L) + \frac{L_m}{2} \dot{v}_x(t, L) + \left( L + \frac{L_m}{2} \right) \dot{\omega}(t) \right] + f(t) \right) \phi(L) \\
& - \frac{L_m}{2} \left( m \left[ \dot{v}(t, L) + \frac{L_m}{2} \dot{v}_x(t, L) + \left( L + \frac{L_m}{2} \right) \dot{\omega} \right] + f(t) \right) \phi_x(L) \\
& + J_1 (\dot{v}_x + \dot{\omega}) \phi_x(L) - \frac{L_m}{2} f(t) \phi_x(L) = 0, \tag{A.9}
\end{aligned}$$

equations governing the hub physics,

$$J_0 \dot{\omega}(t) = \gamma I(0) v_{xx}(t, 0) + E I(0) d_{xx}(t, 0) + u(t) - n_0 \omega,$$

and two equations created by the first order substitution,

$$\int_0^L \dot{d} \phi dx = \int_0^L v \phi dx \quad (\text{A.10})$$

$$\dot{\theta}(t) = \omega(t). \quad (\text{A.11})$$

We now introduce the following series approximations to the continuous functions found in equations (A.9) - (A.11):

$$\begin{aligned} d_N(t, x) &= \sum_{j=1}^N a_j(t) \phi_j(x) \quad , \quad v_N(t, x) = \sum_{j=1}^N b_j(t) \phi_j(x) \\ (\dot{v}_N)(t, x) &= \sum_{j=1}^N \dot{b}_j(t) \phi_j(x) \quad , \quad (\dot{v}_N)_x(t, x) = \sum_{j=1}^N \dot{b}_j(t) \phi'_j(x). \end{aligned} \quad (\text{A.12})$$

Substituting the approximations from (A.12) into the integral terms of equation (A.9), approximating  $\phi(x)$  with  $\phi(x) = \phi_i(x)$ , and simplifying while grouping terms yields

$$\begin{aligned} \sum_{j=1}^N \left[ \int_0^L (\rho(x)A(x))\phi_j(x)\phi_i(x) dx \right] \dot{b}_j + \left[ \int_0^L x\phi_i(x) dx \right] \dot{\omega} + \\ \sum_{j=1}^N \left[ \int_0^L (\gamma(x)I(x))\phi''_j(x)\phi''_i(x) dx \right] b_j + \left[ \int_0^L E(x)I(x)\phi''(x) dx \right] a_j \\ + BC \text{ terms}, \quad i = 1 \dots N. \end{aligned} \quad (\text{A.13})$$

Simultaneously performing the same substitutions in the additive boundary condition terms in equation (A.9) and grouping like terms in  $\dot{b}$ ,  $\dot{\omega}$ , and  $f(t)$ , we find

$$\begin{aligned} \left( m M_1 + m \frac{L_m}{2} + J_1 M_3 - m \frac{L_m}{2} M_4 - m \left( \frac{L_m}{2} \right)^2 M_3 \right) \dot{b}(t) \\ + \left( m \left( 1 + \frac{L_m}{2} \right) \phi(L) + J_1 \phi'(L) - m \frac{L_m}{2} \left( L + \frac{L_m}{2} \right) \phi'(L) \right) \dot{\omega}(t) \\ + \left( \phi(L) - \frac{L_m}{2} \phi'(L) \right) f(t), \end{aligned} \quad (\text{A.14})$$

where the matrices  $M_1$ - $M_4$  are defined as:

$$\begin{aligned} [M_1]_{\{ij\}} &= \phi_i(L)\phi_j(L) & [M_2]_{\{ij\}} &= \phi'_i(L)\phi_j(L) \\ [M_3]_{\{ij\}} &= \phi'_i(L)\phi'_j(L) & [M_4]_{\{ij\}} &= \phi_i(L)\phi'_j(L). \end{aligned} \quad (\text{A.15})$$

Constructing new matrix  $M_m$ , and vectors  $w_m$  and  $F_m$  as

$$\begin{aligned} M_m &= \left( m M_1 + m \frac{L_m}{2} + J_1 M_3 - m \frac{L_m}{2} M_4 - m \left( \frac{L_m}{2} \right)^2 M_3 \right) \\ w_m &= \left( m \left( 1 + \frac{L_m}{2} \right) \phi(L) + J_1 \phi'(L) - m \frac{L_m}{2} \left( L + \frac{L_m}{2} \right) \phi'(L) \right) \\ F_m &= \left( \phi(L) - \frac{L_m}{2} \phi'(L) \right), \end{aligned}$$

the dynamics resulting from the boundary conditions in equations (A.13) - (A.14) can thus be written in matrix-vector form as

$$M_m \dot{b}(t) + w_m \dot{\omega}(t) + F_m f(t). \quad (\text{A.16})$$

Furthermore, let

$$\begin{aligned} M_{ij} &= \left[ \int_0^L (\rho(x)A(x)) \phi_j(x)\phi_i(x) dx \right], & D_{ij} &= \left[ \int_0^L (\gamma(x)I(x)) \phi_j''(x)\phi_i''(x) dx \right] \\ K_{ij} &= \left[ \int_0^L E(x)I(x) \phi''(x) dx \right], & n_i &= \left[ \int_0^L x\phi_i(x) dx \right], \end{aligned} \quad (\text{A.17})$$

and

$$\begin{aligned} M_s &= M + M_m \\ n_s &= n + w_m. \end{aligned}$$

The matrix form of equation (A.13), including boundary condition dynamics terms,

can then be written as

$$M_s \dot{b}(t) + n_s \dot{\omega}(t) = -D b(t) - K a(t) - F_m f(t).$$

Equation A.8 becomes

$$J_0 \dot{\omega} = \sum_{j=1}^N [E(0)I(0)\phi_j''(0)] a_j + [\gamma(0)I(0)\phi_j''(0)] b_j + u(t) - n_0 \omega.$$

Let

$$q = E(0)I(0)\phi''(0) , r = \gamma(0)I(0)\phi''(0),$$

then

$$J_0 \dot{\omega} = q^T a + r^T b + u(t) - n_0 \omega,$$

where  $T$  denotes vector transpose. Following the same substitution procedure, equation (A.10) becomes

$$\sum_{j=1}^N \left[ \int_0^L \phi_j \phi_i dx \right] \dot{a}_j = \sum_{j=1}^N \left[ \int_0^L \phi_j \phi_i dx \right] b_j.$$

Let  $M^0$  be the matrix with  $ij$  components

$$M_{ij}^0 = \left[ \int_0^L \phi_j(x) \phi_i(x) dx \right],$$

then

$$\begin{aligned} \sum_{j=1}^N M_{ij}^0 \dot{a}_j &= \sum_{j=1}^N M_{ij}^0 b_j \\ M_{ij}^0 \dot{a}_j &= M_{ij}^0 b_j \\ \dot{a}_j &= b_j. \end{aligned}$$

Thus we obtain the finite element differential equations

$$\begin{aligned}
 M_s \dot{b} + n_s \dot{\omega} &= -D b - K a \\
 J \dot{\omega} &= q^T a + r^T b + u(t) - n_0 \omega \\
 \dot{a}_j &= b_j \\
 \dot{\theta} &= \omega.
 \end{aligned} \tag{A.18}$$

The above can be represented in state space form as

$$\begin{bmatrix} I & 0 & 0 & 0 \\ 0 & M_s & 0 & n_s \\ 0 & 0 & 1 & 0 \\ 0 & 0 & 0 & J \end{bmatrix} \begin{bmatrix} \dot{a} \\ \dot{b} \\ \dot{\theta} \\ \dot{\omega} \end{bmatrix} = \begin{bmatrix} 0 & I & 0 & 0 \\ -K & -D & 0 & 0 \\ 0 & 0 & 0 & 1 \\ q^T & r^T & 0 & -n_0 \end{bmatrix} \begin{bmatrix} a \\ b \\ \theta \\ \omega \end{bmatrix} + \begin{bmatrix} 0 \\ 0 \\ 0 \\ 1 \end{bmatrix} u(t) + F_m f(t). \tag{A.19}$$

Let  $z$  be the column vector

$$z = \begin{bmatrix} a \\ b \\ \theta \\ \omega \end{bmatrix}, \tag{A.20}$$

and

$$M_{sys} = \begin{bmatrix} I & 0 & 0 & 0 \\ 0 & M_s & 0 & n_s \\ 0 & 0 & 1 & 0 \\ 0 & 0 & 0 & J \end{bmatrix}, A_{sys} = \begin{bmatrix} 0 & I & 0 & 0 \\ -K & -D & 0 & 0 \\ 0 & 0 & 0 & 1 \\ q^T & r^T & 0 & -n_0 \end{bmatrix}, \quad (\text{A.21})$$

$$B_{sys} = \begin{bmatrix} 0 \\ 0 \\ 0 \\ 1 \end{bmatrix}. \quad (\text{A.22})$$

Equation (A.19) can then be written as

$$\dot{z} = [M_{sys}^{-1} A_{sys}] z + [M_{sys}^{-1} B_{sys}] u(t) + [M_{sys}^{-1} F_m] f(t), \quad (\text{A.23})$$

or, in more compact notation,

$$\dot{z} = A z + B u(t) + F f(t) \quad (\text{A.24})$$

$$y = C z. \quad (\text{A.25})$$

Where the matrix  $C$  is determined by what states we are able to sense. This matrix will take one of two forms throughout the discussion. In the first form, only hub angular position and velocity are sensed.  $C$  would then be a  $2 \times (2N + 2)$  matrix where  $N$  is the number of finite element nodes chosen, and has the form:

$$C = \begin{bmatrix} \text{zeros}(1, 2N) & 1 & 0 \\ \text{zeros}(1, 2N) & 0 & 1 \end{bmatrix}, \quad (\text{A.26})$$

where the ones appear in the hub position and hub velocity state positions. A  $C$  matrix that corresponds to the sensed state of beam tip velocity, resulting from placement of an accelerometer at the beam tip, would take the form of the following  $3 \times (2N + 2)$  matrix:

$$C = \begin{bmatrix} \text{zeros}(1, N) & \phi(L) & 0 & 0 \\ \text{zeros}(1, N) & \text{zeros}(1, N) & 1 & 0 \\ \text{zeros}(1, 2N) & 0 & 1 & \end{bmatrix}. \quad (\text{A.27})$$

Recall that  $\phi(L)$  is a vector with  $i$ th entry  $\phi_i(L)$ , corresponding to the basis function values at those nodes.

## B SIMULATIONS

This is a compilation of all simulations performed that were used or mentioned in this thesis. They are grouped in the following manner.

- Uncontrolled
  - Uncontrolled Aluminum
  - Uncontrolled Bone
  - Uncontrolled Aluminum with Disturbance
  - Uncontrolled Bone with Disturbance
- Regulation
  - Bone with Disturbance
- Tracking
  - Bone with Disturbance

## Aluminum - No Disturbance

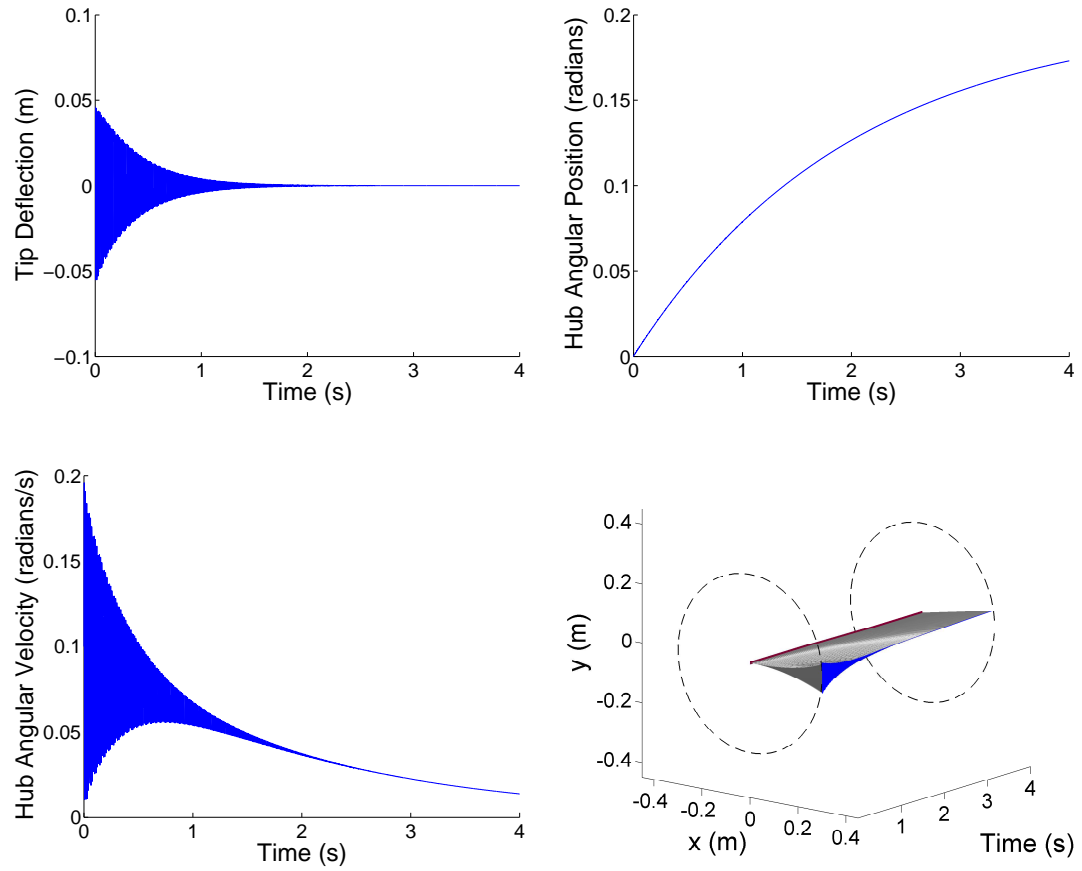


Figure B.1: Uncontrolled aluminum undisturbed

## Bone - No Disturbance

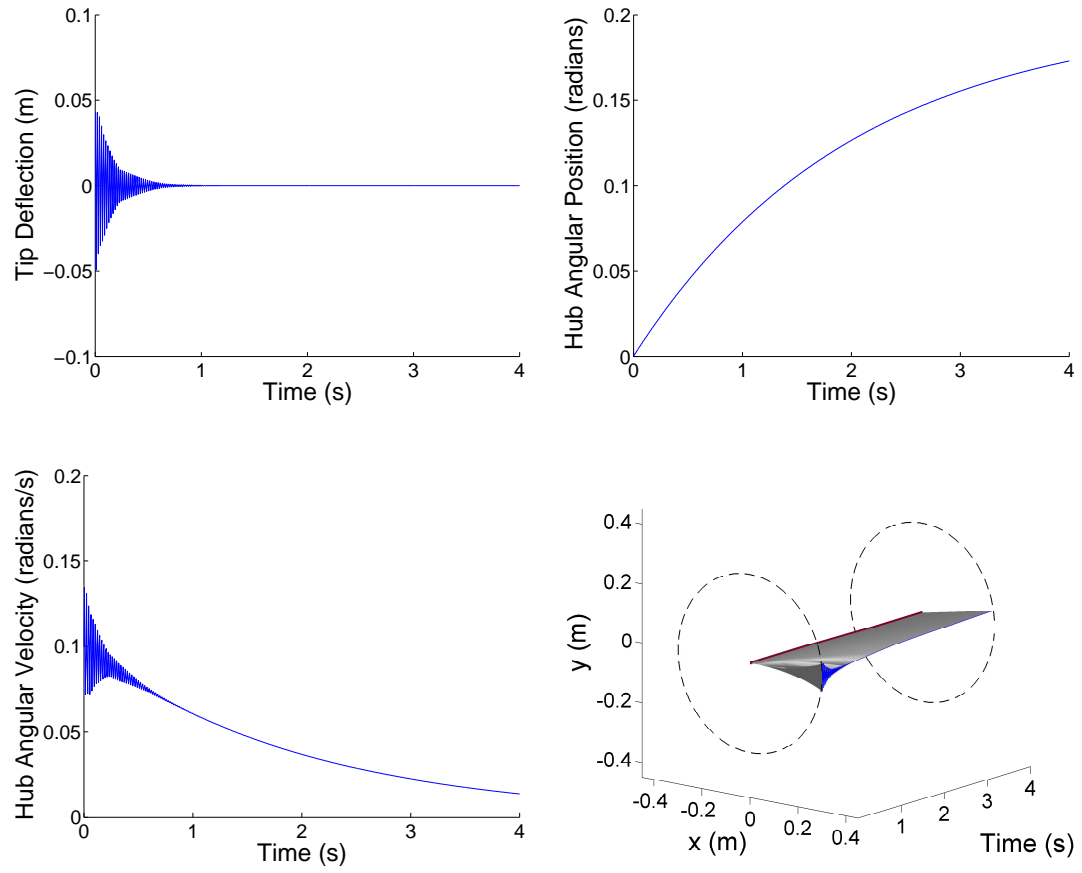


Figure B.2: Uncontrolled bone undisturbed

## Aluminum - Disturbance

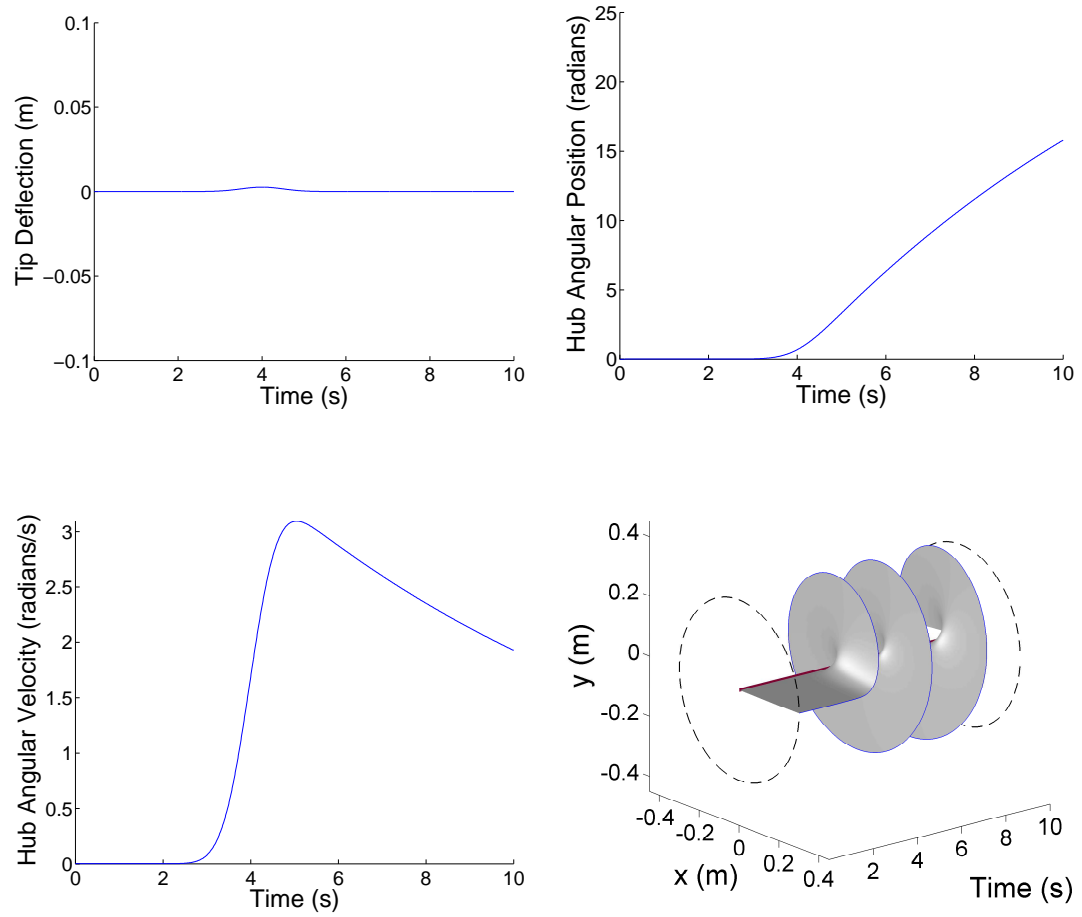


Figure B.3: Uncontrolled aluminum disturbed

## Bone - Disturbance

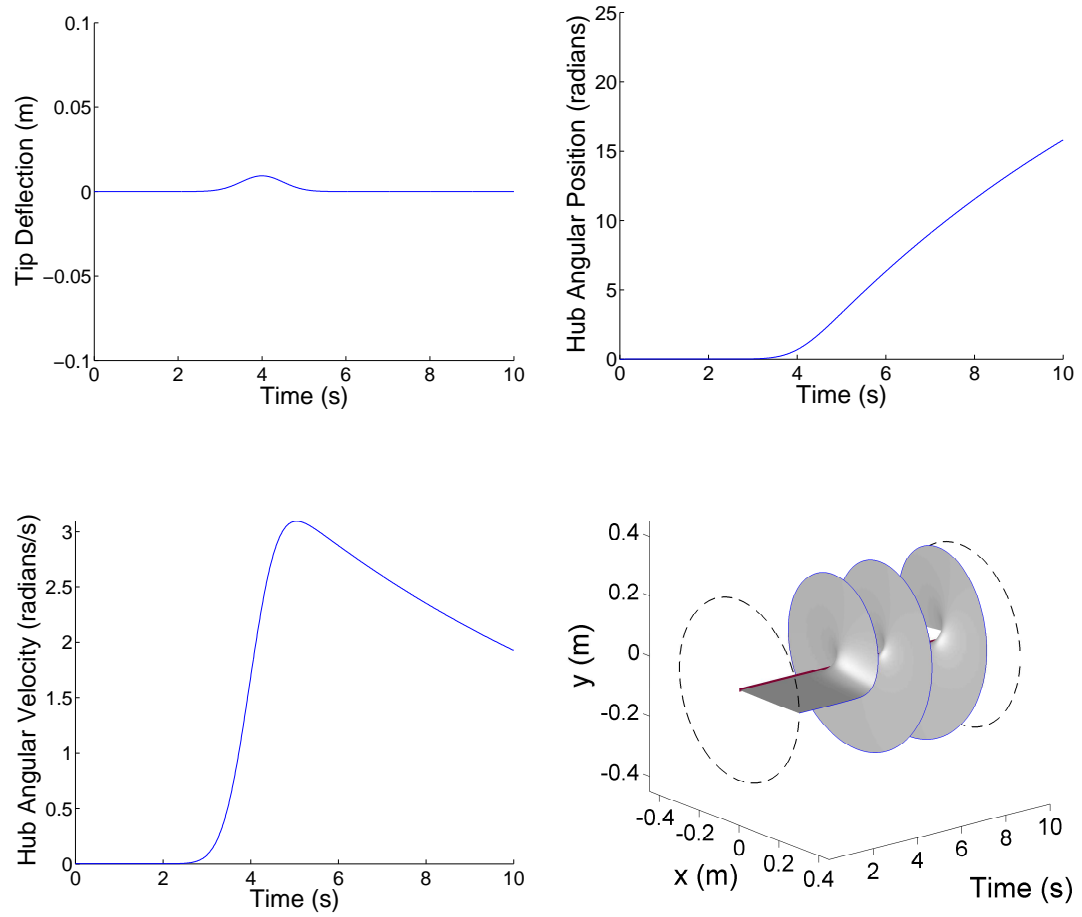


Figure B.4: Uncontrolled bone disturbed

Regulation  
Bone - Disturbance

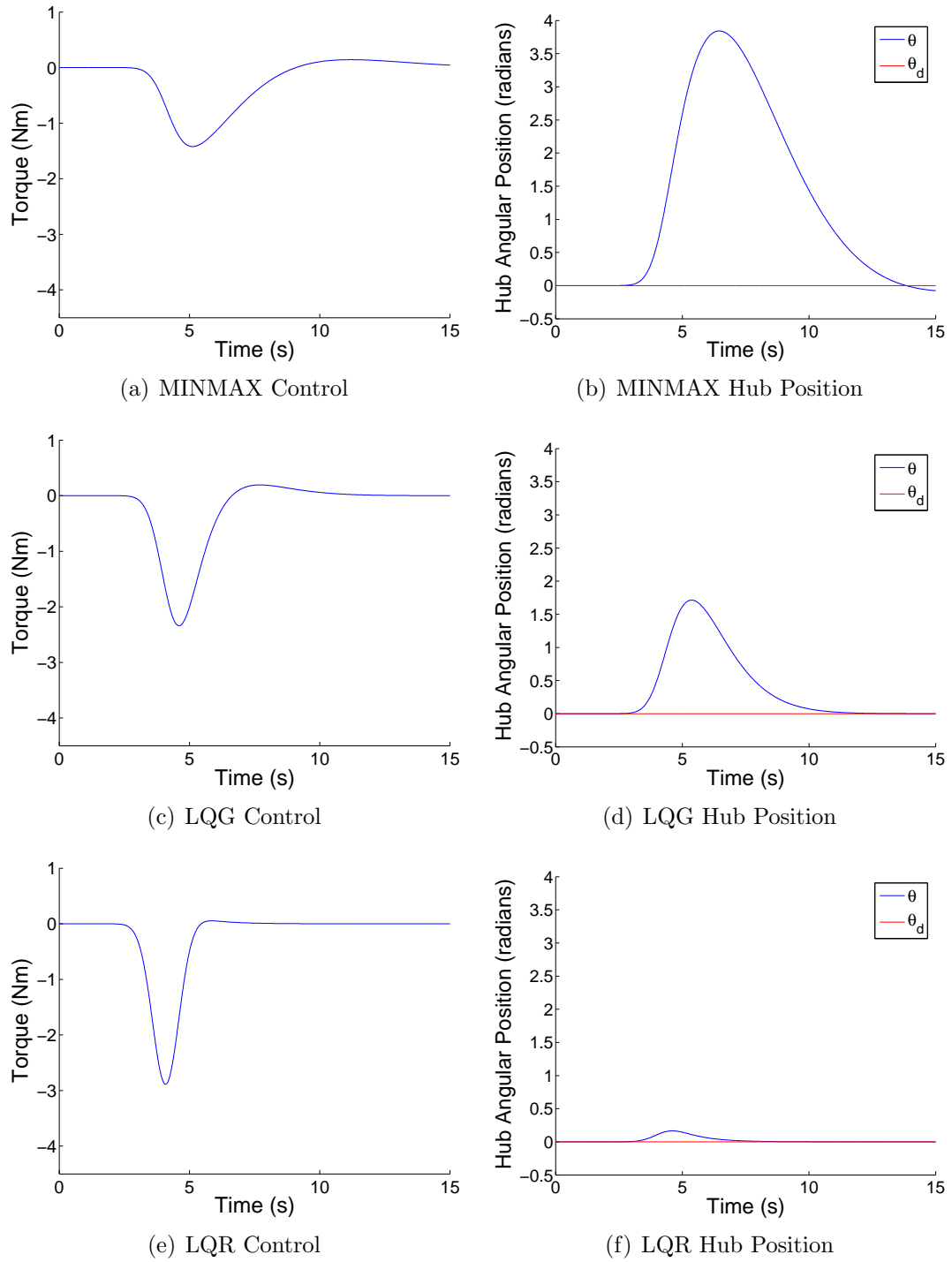


Figure B.5: Regulation bone disturbed - Control and hub position

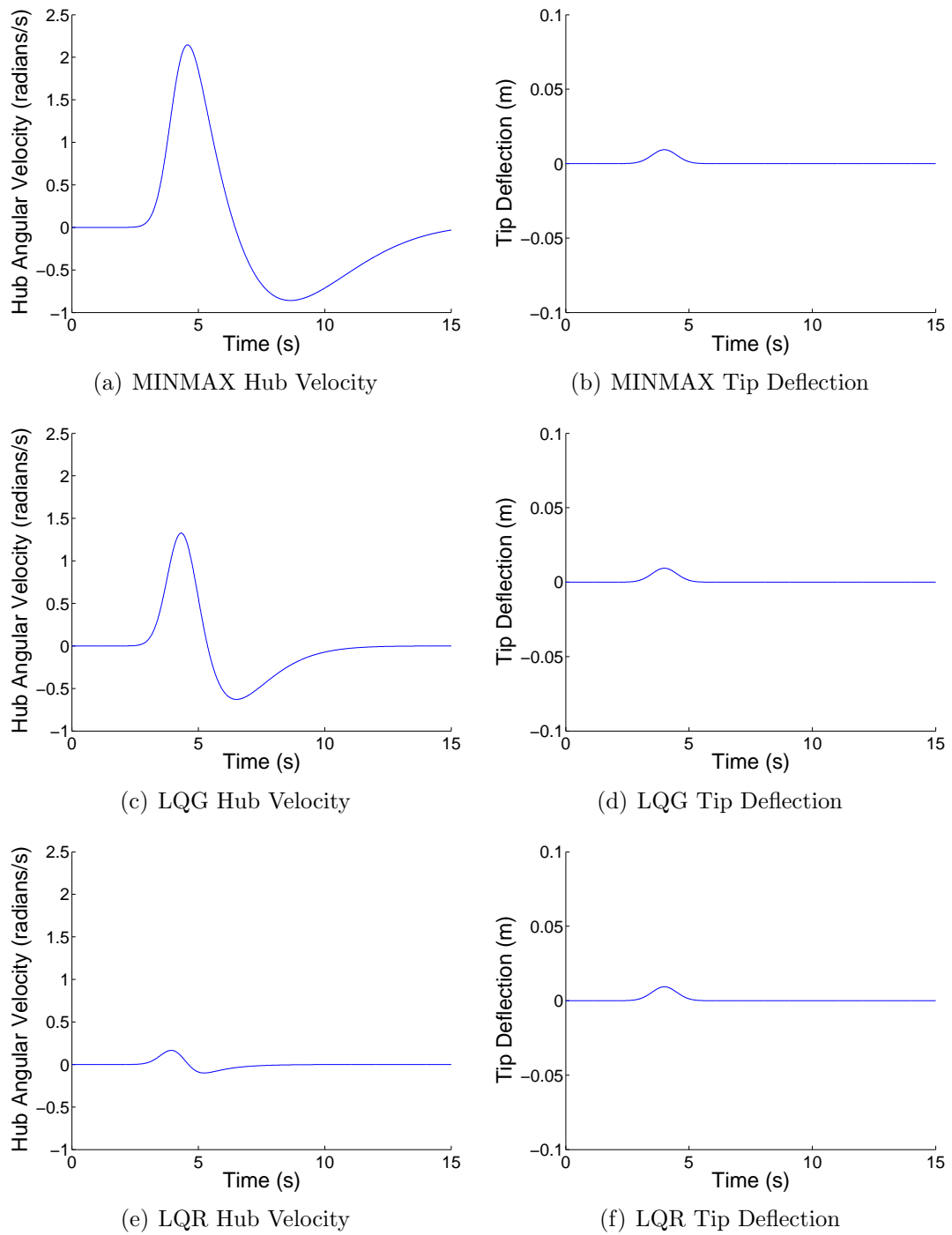


Figure B.6: Regulation bone disturbed - Hub velocity and tip deflection

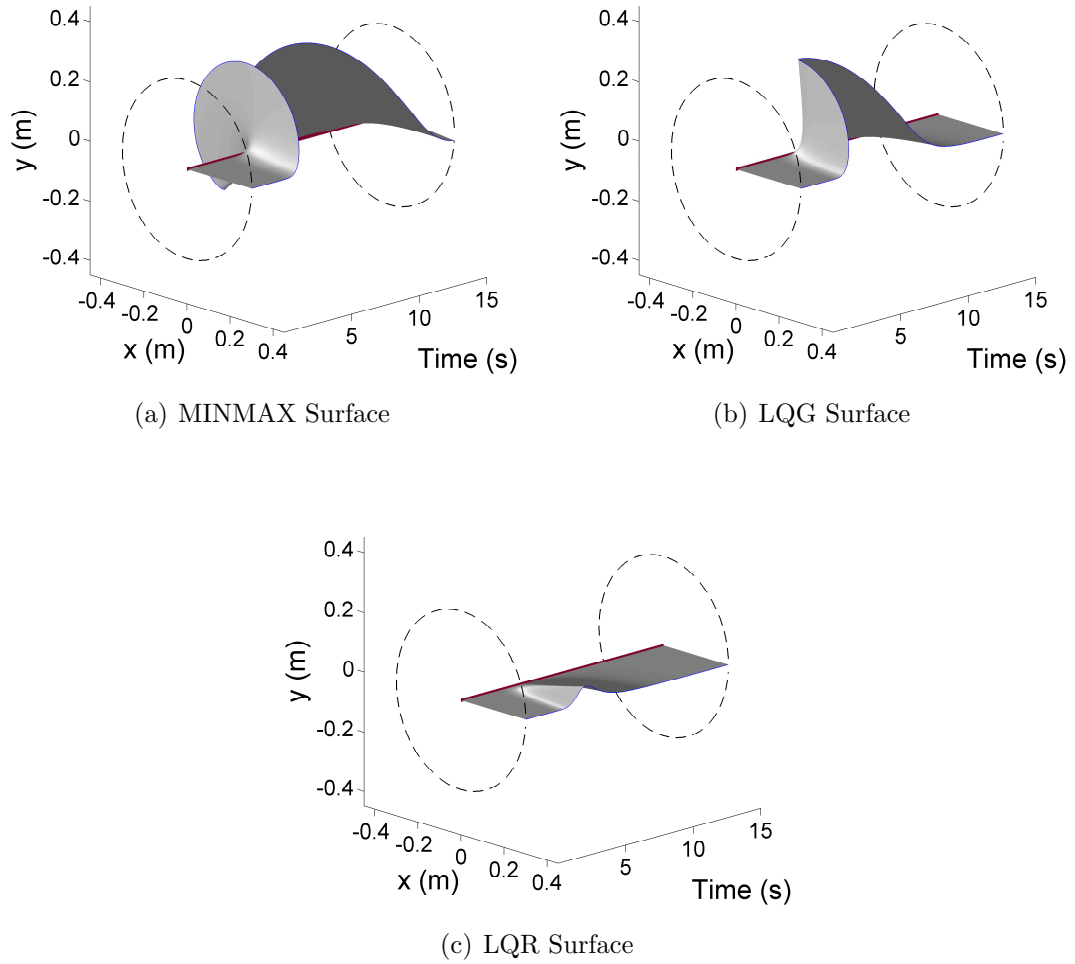


Figure B.7: Regulation bone disturbed - Surface plot

Tracking  
Bone - Disturbance

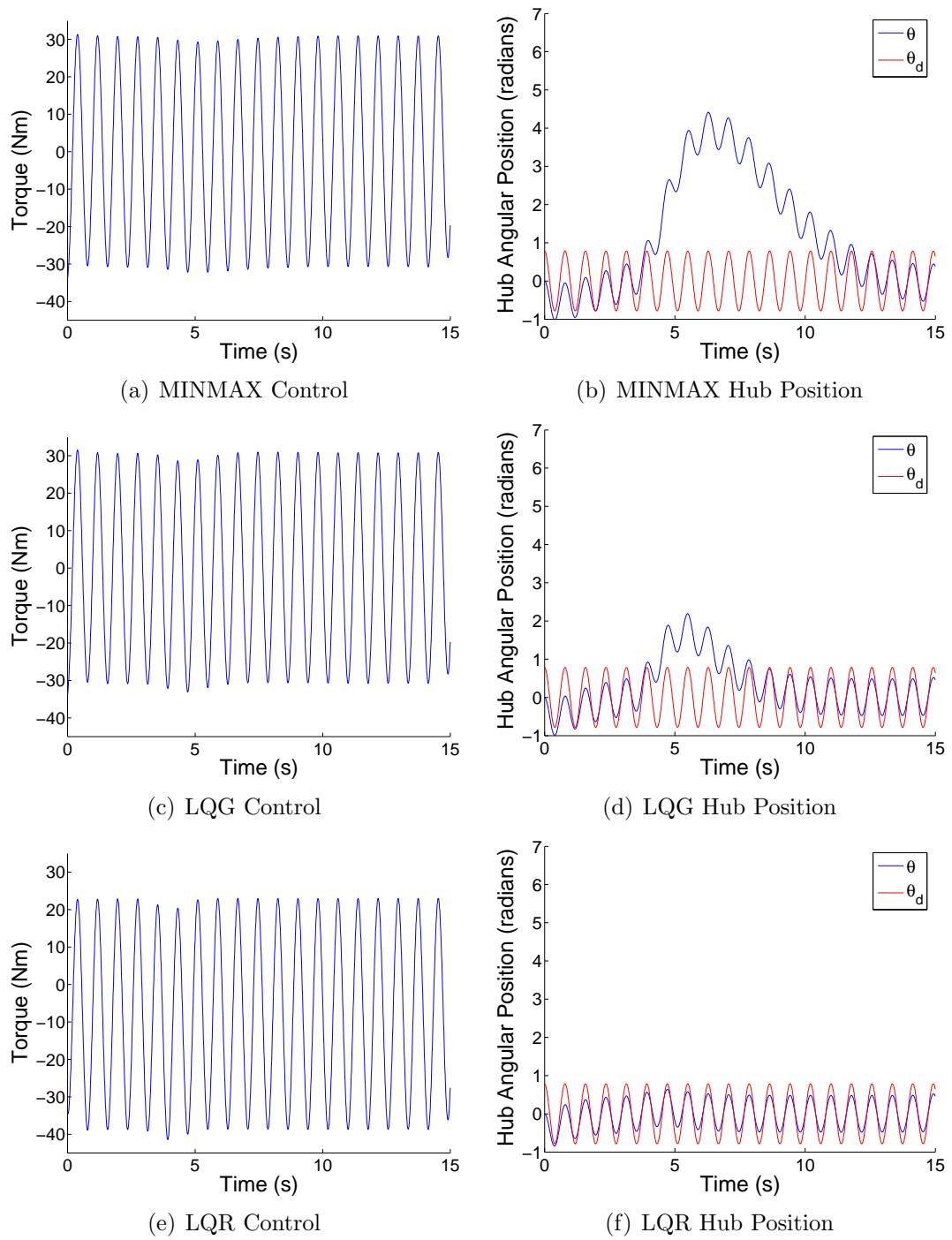


Figure B.8: Tracking/disturbed: Bone beam control and hub position

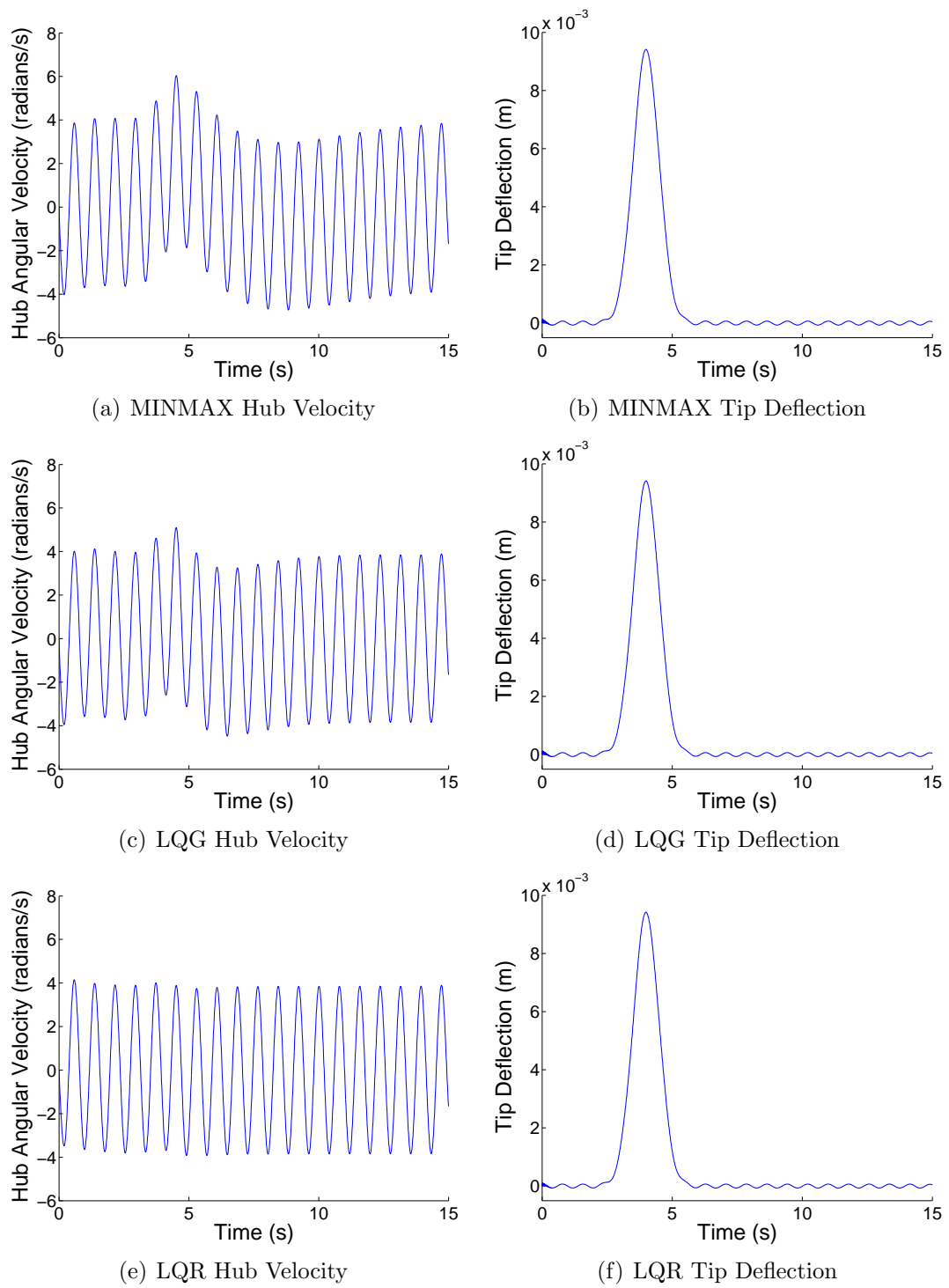
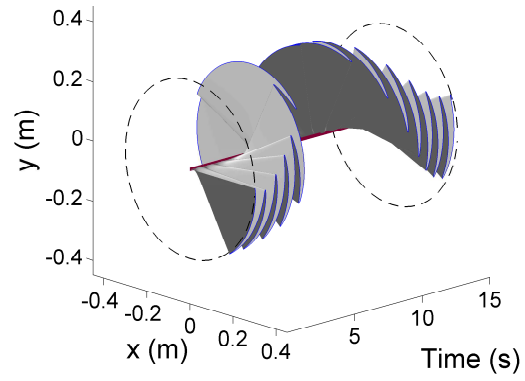
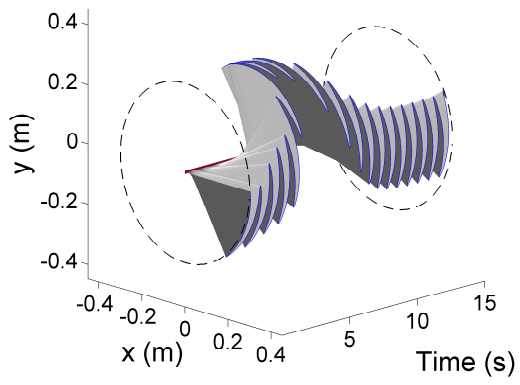


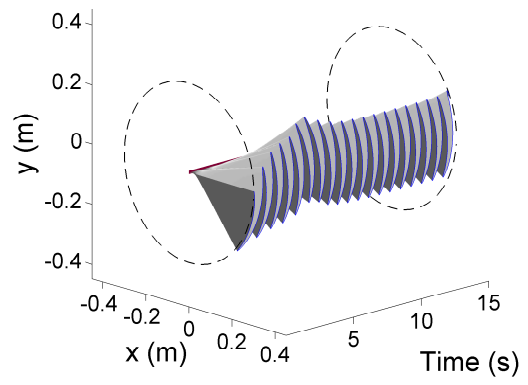
Figure B.9: Tracking/disturbed: Bone beam hub velocity and tip deflection



(a) MINMAX Surface



(b) LQG Surface



(c) LQR Surface

Figure B.10: Tracking/disturbed: Surface plots